



HAL
open science

Synthesis, characterization and biological application of four novel metal-Schiff base complexes derived from allylamine and their interactions with human serum albumin: Experimental, molecular docking and ONIOM computational study

Zahra Kazemi, Hadi Amiri Rudbari, Mehdi Sahihi, Valiollah Mirkhani, Majid Moghadam, Shahram Tangestaninejad, Iraj Mohammadpoor-Baltork, Sajjad Gharaghani

► To cite this version:

Zahra Kazemi, Hadi Amiri Rudbari, Mehdi Sahihi, Valiollah Mirkhani, Majid Moghadam, et al.. Synthesis, characterization and biological application of four novel metal-Schiff base complexes derived from allylamine and their interactions with human serum albumin: Experimental, molecular docking and ONIOM computational study. *Journal of Photochemistry and Photobiology B: Biology*, 2016, 162, pp.448-462. 10.1016/j.jphotobiol.2016.07.003 . hal-04087621

HAL Id: hal-04087621

<https://uca.hal.science/hal-04087621>

Submitted on 3 May 2023

HAL is a multi-disciplinary open access archive for the deposit and dissemination of scientific research documents, whether they are published or not. The documents may come from teaching and research institutions in France or abroad, or from public or private research centers.

L'archive ouverte pluridisciplinaire **HAL**, est destinée au dépôt et à la diffusion de documents scientifiques de niveau recherche, publiés ou non, émanant des établissements d'enseignement et de recherche français ou étrangers, des laboratoires publics ou privés.



Distributed under a Creative Commons Attribution - NonCommercial - NoDerivatives 4.0 International License

Synthesis, characterization and biological application of four novel metal-Schiff base complexes derived from allylamine and their interactions with human serum albumin: Experimental, molecular docking and ONIOM computational study

Zahra Kazemi ^a, Hadi

Amiri Rudbari ^a, Mehdi Sahihi ^a, Valiollah Mirkhani ^a, Majid Moghadam ^a, Shahram Tangestani nejad ^a, Iraj Mohammadpoor-Baltork ^a, Sajjad Gharaghani ^b

^a

Department of Chemistry, University of Isfahan, Isfahan 81746-73441, Iran

^b

Department of Bioinformatics, Laboratory of Chemoinformatics, Institute of Biochemistry and Biophysics, University of Tehran, Tehran, Iran

Abstract

Novel metal-based drug candidate including **VOL₂**, **NiL₂**, **CuL₂** and **PdL₂** have been synthesized from 2-hydroxy-1-allyliminomethyl-naphthalen ligand and have been characterized by means of elemental analysis (CHN), FT-IR and UV-vis spectroscopies. In addition, ¹H and ¹³C NMR techniques were employed for characterization of the **PdL₂** complex. Single-crystal X-ray diffraction technique was utilized to characterise the structure of the complexes. The Cu(II), Ni(II) and Pd(II) complexes show a square planar trans-coordination geometry, while in the **VOL₂**, the vanadium center has a distorted tetragonal pyramidal N₂O₃ coordination sphere. The HSA-binding was also determined, using fluorescence quenching, UV-vis spectroscopy, and circular dichroism (CD) titration method. The obtained results revealed that the HSA affinity for binding the synthesized compounds follows as **PdL₂** > **CuL₂** > **VOL₂** > **NiL₂**, indicating the effect of metal ion on binding constant. The distance between these compounds and HSA was obtained based on the Förster's theory of non-radiative energy transfer. Furthermore, computational methods including molecular docking and our Own N-layered Integrated molecular Orbital and molecular Mechanics (ONIOM) were carried out to investigate the HSA-binding of the compounds. Molecular docking calculation indicated the existence of hydrogen bond between amino acid residues of HSA and all synthesized compounds. The formation of the hydrogen bond in the HSA-compound systems leads to their stabilization. The ONIOM method

was utilized in order to investigate HSA binding of compounds more precisely in which molecular mechanics method (UFF) and semi empirical method (PM6) were selected for the low layer and the high layer, respectively. The results show that the structural parameters of the compounds changed along with binding to HSA, indicating the strong interaction between the compounds and HSA. The value of binding constant depends on the extent of the resultant changes. This should be mentioned that both theoretical methods calculated the K_b values in the same sequence and are in a good agreement with the experimental data.

Keywords

Schiff base compounds

Crystal structure

HSA binding

Molecular modelling

ONIOM calculations

1. Introduction

The compounds containing azometine group (Schiff base) are of compounds that fascinate a large number of chemists and biochemists [1], [2], [3] due to their easy formation, high stability, their pharmacological properties and notably anticancer activity [4]. The researches have revealed that the bioactivity of many ligands significantly enhances by complexation to a metal ion. Transition metal complexes can possess various molecular geometries by changing coordination number that is not achievable for purely organic molecule. Their tunable properties such as oxidation states are another advantage [2]. Furthermore, since discovery of Platinum-based anticancer drugs (cisplatin, carboplatin and oxaliplatin) as potent chemotherapeutic agents and then diagnose their drawbacks (drug resistance, normal tissue toxicity, nephrotoxicity and neurotoxicity) a growing interest in synthesis non-platinum metal complexes as a drug has been revealed [5], [6].

Some metal ions such as Copper [7], Palladium [8], Nickel [9] and Vanadium [10] have significant biological activity and have been investigated by some workers over the years. Because

of: a) remarkable analogy between Pd(II) and Pt(II) complexes [11]; Palladium complexes are regarded as potential anticancer substances that in some cases they have better anticancer activity than their Pt(II) analogue [12]. b) Less toxicity and higher activity of Cu(II) and Pd(II) complexes in compared to platinum ones. Therefore, Cu(II) complexes are known as good alternative to cisplatin. The significance of Copper in some biological processes and the reliance of catalytic activity of many enzymes on it causes Cu(II) complexes have attracted much attention [12], [13]. c) Promising biological activities of these metal complexes [14], [15], [16] d) novel action mechanism of vanadium by the generation of reactive oxygen species (ROS); Vanadium is capable of increasing the ROS level, promoting apoptosis of cells and inhibiting tumour cell proliferation. Therefore, the cell growth and spread of tumour is suppressed [17]. e) Less investigation of interaction of Ni(II) and V(IV) compounds with biomacromolecules in compared to other metal ions such as Pd(II), Zn(II) and Cu(II), despite the fact that they play vital role in biological systems. Hence, it is essential to synthesis and study the affinity of their complexes to some biomacromolecules.

The knowledge about interaction mechanisms of drug with plasma proteins as a biomacromolecule is required to understand pharmacodynamics and pharmacokinetics of drugs [18]. As regards function of plasma proteins as drug carriers, there are a large number of literatures about binding of drugs to them [19], [20]. Consequently, the interaction of plasma proteins with metal complexes as a drug candidate is worthy of evaluation.

Generally, proteins are known as the major targets for most of the drugs in organisms [21]. Their interaction with drug affects on the drug absorption, distribution and elimination in the circulatory system [22], and can prevent their rapid elimination from blood stream [23]. Human serum albumin (HSA) is the most abundant plasma protein, it also is known as the dominant transporter plasma protein for endogenous and exogenous ligands (fatty acids, hormones and drugs) [24]. The accommodation of a wide range of lipophilic molecules in HSA is possible as a result of its flexible structure [25]. The HSA-binding of drug can increase its solubility in plasma, decrease its toxicity, protect from oxidation, prolong its in vivo half-life as well as increase the pharmaceutical effect of drug [26]. Fig. 1 shows the way of HSA-binding of a metal complex: This interaction can be occurred through the donor atoms of ligands (the first coordination sphere), or with more remote located groups on the ligands (the second coordination sphere) [27].

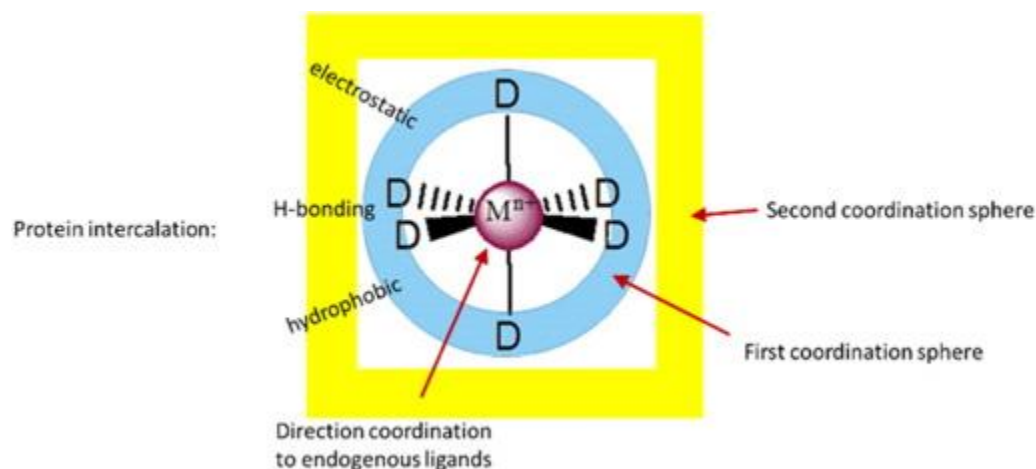


Fig. 1. Schematic illustration of non-covalent interactions of protein with a metal complex (M^{n+} = transition metal, D = donor atoms of exogenous ligands).

In order to obtain information about HSA-binding of drugs ongoing development of accurate computational methods has been observed. Generally the researchers can receive reliable information such as geometries, energies and electronic properties using quantum mechanical (QM) methods. However, the use of purely QM method to calculate the structure of macromolecules is extremely time consuming. Many efforts of researchers led to initiation of hybrid methods and then QM/MM method. Despite the fact that HSA-binding study of drugs with both docking and ONIOM (our own N-layered Integrated molecular Orbital and molecular Mechanics) is feasible, the use of them are rarely seen in literatures [28].

In the current study, V(IV), Ni(II) Cu(II) and Pd(II) ions have been selected for synthesis of new metal complexes. Aware of the therapeutic activity of Schiff base metal complexes and in attempt to obtain more insight into their biological activity, the HSA-binding of the synthesized compounds have been investigated. The experimental methods including fluorescence quenching and UV-vis spectroscopies have been used to evaluate binding behaviour of the synthesized metal complexes to HSA, quantitatively. Secondary structural changes of HSA have been studied using circular dichroism (CD). In addition, to find out appropriate orientation of them into the binding site of HSA, two powerful computational methods, molecular docking and ONIOM have been used.

2. Experimental

2.1. Chemicals and Instrumentation

Human serum albumin (HSA) was purchased from Sigma-Aldrich. 2-Hydroxy-1-naphthaldehyde and allylamine were obtained from Merck Co. and used without further purification. All salts used for buffer preparation were analytical grade and dissolved in double distilled water. All of the solutions were used freshly after preparation. The FT-IR spectra were recorded on a JASCO, FT/IR-6300 spectrometer ($4000\text{--}400\text{ cm}^{-1}$) in KBr pellets. ^1H and ^{13}C NMR spectra were recorded on a Bruker Avance 400 spectrometer using DMSO as a solvent for the Palladium(II) complex. The elemental analysis was performed on Leco, CHNS-932 and Perkin-Elmer 7300 DV elemental analyzers. The UV-vis spectra were recorded on a JASCO V-670 spectrophotometer. Fluorescence measurements were carried out on Shimadzu RF-5000 spectrofluorometer at room temperature. The circular dichroism (CD) spectra were recorded using Aviv spectropolarimeter model 215 (Proterion Corp., USA) at $25\text{ }^\circ\text{C}$. The scan speed was 20 nm min^{-1} . The CD spectra were recorded in the far-UV region ($190\text{--}260\text{ nm}$) using 0.1 cm path length cell.

2.2. Preparation of Complexes

2.2.1. General Synthesis

Methanolic solution (10 ml) of 2-hydroxy-1-naphthaldehyde (5 mmol) was added dropwise to a methanolic solution (10 ml) of allylamine (5 mmol). After continuously stirred for 2 h in ambient temperature, solution of triethylamine (7 mmol) in absolute methanol (5 ml) was added to the solution. The mixture was stirred for 10 min , and then a solution of appropriate metal salt ($2.5\text{ mmol NiCl}_2\cdot 6\text{H}_2\text{O}$, $\text{CuCl}_2\cdot 2\text{H}_2\text{O}$, PdCl_2 and $\text{VO}(\text{acac})_2$ salts) in absolute methanol (20 cm^3) was added. The resulting solution was stirred for 2 h at ambient temperature for the preparation of VOL_2 , NiL_2 and CuL_2 complexes, while for Palladium(II) complex, the solution was refluxed overnight to proceed completely.

2.2.2. Copper(II) Complex CuL_2

Dark green crystals were collected by filtration. The green flat crystals were obtained in chloroform by recrystallization. The typical yield was 87% . Anal. calc. for $\text{C}_{28}\text{H}_{24}\text{CuN}_2\text{O}_2$: C:

69.48, H: 5.0, N: 5.79. Found: C: 69.33, H: 4.67, N: 5.28. Selected IR data (KBr, cm^{-1}): 1611 ($\nu\text{C-N}$), 1459 ($\nu\text{C-N}$), 1365 ($\nu\text{C-O}$).

N), 1459 ($\nu\text{C-N}$), 1365 ($\nu\text{C-O}$).

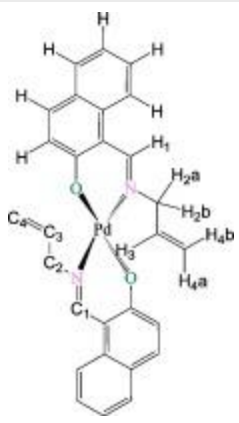
2.2.3. Palladium(II) Complex PdL₂

The resulting green powder was isolated by filtration and washed by dry methanol several times. Then an appropriate single crystal for X-ray crystallography was obtained by dissolving in DMSO and diethylether diffusion. The typical yield was 61%. Anal. calc. for C₂₈H₂₄PdN₂O₂: C: 63.82, H:

4.59, N: 5.32. Found: C: 69.83, H: 5.38, N: 5.41. Selected IR data (KBr, cm^{-1}): 1612 ($\nu\text{C-N}$),

1434 ($\nu\text{C-N}$), 1361 ($\nu\text{C-O}$). ¹HNMR and ¹³CNMR: Table 1.

Table 1. ¹H NMR and ¹³C NMR data for PdL₂.

	¹ H NMR		¹³ C NMR	
	Label	Chemical Shift (ppm)	Label	Chemical Shift (ppm)
H ₁	8.8(s)	C ₁	164.1	
H _{2a} , H _{2b}	4.6(d)	C ₂	58.5	
H ₃	6.1(m)	C ₃	137.1	
H _{4a}	5.2(d)	C ₄	110.1	
H _{4b}	5.3(d)	C _{aromatic}	157.9	
H _{aromatic}	8.2(d)		134.8	
	7.8(d)		134.0	
	7.7(d)		128.7	
	7.5(t)		127.4	
	7.3(t)		126.3	

7.1(d)	122.9
	122.2
	119.8
	116.7

s, singlet; d, doublet; t, triplet; m, multiplet.

2.2.4. Nickel(II) Complex NiL₂

The green powder was isolated from the solution and purified by washing with methanol. Then the precipitate was dried at room temperature. The appropriate crystal was obtained in chloroform by recrystallization. The typical yield was 91%. Anal. calc. for C₂₈H₂₄NiN₂O₂: C: 70.18, H: 5.05, N: 5.85. Found: C: 69.91, H: 5.18, N: 5.62. Selected IR data (KBr, cm⁻¹): 1612 (νC=N), 1433 (νC=N), 1366 (νC=O).

2.2.5. Vanadium (II) Complex VOL₂

The resultant clear yellow solution was allowed to stand overnight. After concentration at room temperature, dark yellow precipitate was collected by filtration. Appropriate single crystals for X-ray crystallography were obtained directly from the reaction mixture. The typical yield was 78%. Anal. calc. for C₂₈H₂₄N₂O₃V: C: 68.99, H: 4.96, N: 5.75. Found: C: 68.82, H: 4.32, N: 5.91. Selected IR data (KBr, cm⁻¹): 1603 (νC=N), 1455 (νC=N), 1359 (νC=O).

2.3. Single Crystal Diffraction Studies

X-ray data for VOL₂, NiL₂, CuL₂ and PdL₂ complexes were collected on a STOE IPDS-II diffractometer with graphite monochromated Mo-Kα radiation. Suitable crystal was chosen using a polarizing microscope and they were mounted on a glass fiber which was used for data collection. Cell constants and an orientation matrix for data collection were obtained by least-squares refinement of diffraction data. Data were collected at a temperature of 298(2) in a series of ω scans in 1° oscillations and integrated using the Stoe X-AREA [29] software package. A numerical absorption correction was applied using the X-RED [30] and X-SHAPE [31] software's.

The data were corrected for Lorentz and Polarizing effects. The structure was solved by direct methods using SIR2004. The non-hydrogen atoms were refined anisotropically by the full matrix least squares method on F2 using SHELXL [32]. All hydrogen atoms were added at ideal positions and constrained to ride on their parent atoms. Crystallographic data are listed in Table S1. Selected bond distances and angles are summarized in Table S2.

2.4. HSA Binding Experiments

2.4.1. Preparation of Compounds and Protein Solution

A stock solution of HSA was prepared by dissolving the desired amount of HSA in 50 mM phosphate buffer (pH = 7). The HSA stock solution was stored at 4 °C in the dark and used within 2 h. HSA concentration was determined by UV–vis spectrophotometry using the molar absorption coefficient $35,700 \text{ M}^{-1} \text{ cm}^{-1}$ at 278 nm [33]. The solution of the complexes was first prepared in DMSO, and then diluted suitably with phosphate buffer to required concentrations for all the experiments. The volume of DMSO never exceeded 1.5% (v/v), so the effect of DMSO is negligible. All the solutions were used freshly after preparation.

2.4.2. Fluorescence Spectroscopic Measurements

The interaction of HSA with the synthesized Schiff base complexes (V(II), Cu(II), Ni(II) and Pd(II) complexes) was investigated using fluorescence quenching experiment. In this experiment 2 ml of HSA solution (3 μM) was placed into the cell and various amount of the compounds ($5 \times 10^{-5} \text{ M}$) were added to the cell. The fluorescence intensity was measured with excitation wavelength at 295 nm and emission wavelength rang of 300–450 nm. In each measurement the mixture was allowed to incubate for 2 min after addition of the complexes.

2.4.3. UV–vis Absorption Spectroscopy Measurements

Absorption titration experiment, an operational and very easy method, was also carried out to more investigation of HSA-binding of the compounds at room temperature. The UV–vis absorption spectra of the solution of HSA (5 μM) in the absence and presence of various amount of the compounds ($5 \times 10^{-5} \text{ M}$) were recorded. Absorption curves of compounds–protein mixtures were

corrected by subtracting the spectra of compounds solutions. All intensities were corrected for the dilution effect in fluorescence and UV absorption experiments.

2.4.4. Circular Dichroism Spectroscopy

The circular dichroism (CD) spectrum was recorded at room temperature in the range of 190–260 nm, using 0.1 cm quartz cell. The CD spectrum of HSA solution was recorded before and after addition of the synthesized compounds with molar ratio 0, 0.5, 1 and 2. The analysis CD spectra were carried out by CDNN software. The content of secondary conformation of HSA in each step was calculated from this technique. The spectra were obtained by subtracting the spectra of compounds as baseline.

2.4.5. Computational Details

2.4.5.1. Molecular Docking Simulation

In this work, docking study was carried out to indicate the HSA-binding site for the synthesized compounds. The 3D structures of the metal complexes were generated using the CIF files of their X-ray crystal structures. The CIF files were converted to the PDB format by using the Mercury software (<http://www.ccdc.cam.ac.uk/>). The crystal structure of HSA (PDB ID: 1AO6) was taken from the Brookhaven Protein Data Bank (<http://www.rcsb.org/pdb>). The R-value and resolution of this file were 0.218 and 0.25 Å, respectively. It was prepared in pH = 7.5. Water molecules of the protein pdb file were removed, missing hydrogen atoms and Gasteiger charges were added. Flexible-ligand docking was performed by AutoDock 4.2 molecular-docking program using the implemented empirical free energy function and the Lamarckian Genetic Algorithm [34]. The Gasteiger charges were added to prepare the macromolecule input file for docking and the Auto Grid was used to calculate Grids. A blind docking with 126 lattice points along X, Y, and Z axes was performed to find the active site of ligands to the HSA. After determination of the active site, the dimensions of the grid map were selected 60 points with a grid point spacing of 0.375 Å, to allow the ligand to rotate freely. 200 docking runs with 25,000,000 energy evaluations for each run were performed.

2.4.5.2. Quantum Mechanical/Molecular Mechanics (QM/MM) Calculations

Present work investigates the interaction of the compounds with HSA accurately, using QM/MM calculations. In order to carry out QM/MM calculations, our own N-layered Integrated molecular Orbital and molecular Mechanics (ONIOM) methodology was employed. The ONIOM can be considered as a hybrid method, quantum mechanical method (QM) with a molecular mechanics (MM). Although this method was used as a two-layer QM/MM in this study, it is capable of combining any number of molecular orbital and molecular-mechanics methods and extending [35].

This method also is able to apply different ab initio or semi-empirical methods to different parts of a molecule/system and combine to produce reliable geometry and energy at reduced computational time [36]. In the two layers ONIOM method, the total energy (E_{ONIOM}) of the whole system is a sum of the three independent energy calculations: [37]

$$E^{ONIOM2} = E_{\text{model system}}^{\text{high}} + E_{\text{real system}}^{\text{low}} - E_{\text{real system}}^{\text{low}} \quad (1)$$

Real system contains full geometry of the molecule and is considered as MM layer while the model system contains the chemically most important (core) part of the system that is considered as QM layer. Furthermore, the stability of respective adducts was obtained by the evaluation the interaction energy (ΔE), which is calculated by the following equation:

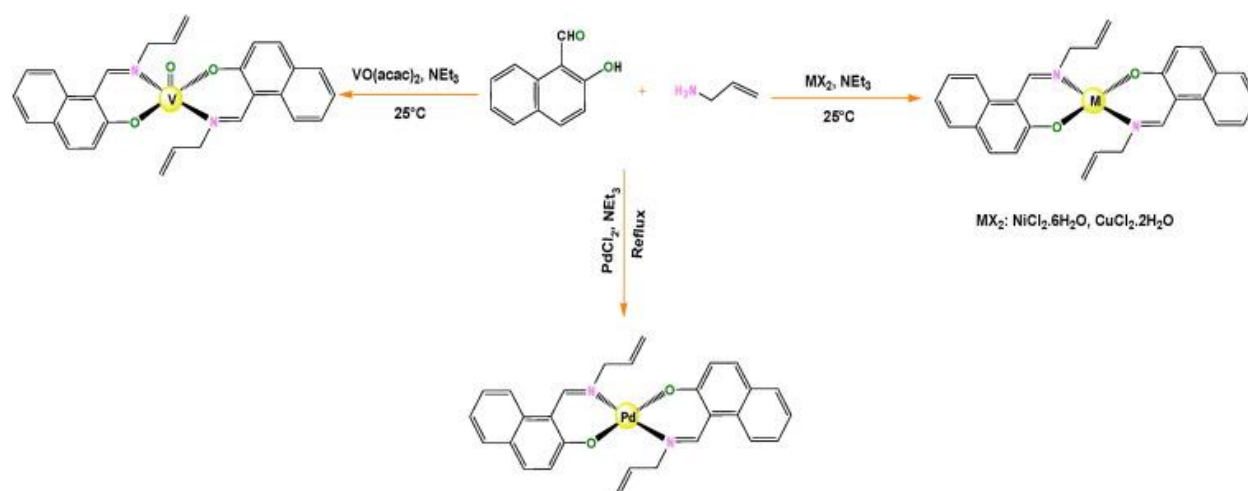
$$\Delta E = \Delta E_{\text{HSA /compound}} - \Delta E_{\text{HSA}} - \Delta E_{\text{compound}} \quad (2)$$

where $\Delta E_{\text{HSA/compound}}$, ΔE_{HSA} and $\Delta E_{\text{compound}}$ are the energy of the optimized adduct of compound-HSA, HSA receptor and compounds, respectively. A two layers QM/MM method was opted for all calculations. HSA is considered as low layer while the compounds are considered as high layer in the current work. Molecular mechanics method (UFF) and semi empirical method (PM6) were selected for the low layer and the high layer, respectively.

3. Result and Discussion

3.1. Synthesis and Characterization

The synthesis of Vanadium(IV), Copper(II), Nickel(II) and Palladium(II) Schiff base complexes was carried out by the same route in which $\text{VO}(\text{acac})_2$, CuCl_2 , NiCl_2 and PdCl_2 were treated with two molar equivalents of the ligand in the presence of triethylamine, respectively. All complexes were obtained at room temperature except Pd(II) one that was in reflux condition (Scheme 1). They were characterized by elemental analysis (CHN) and FT-IR spectroscopy. Moreover, the Schiff base Palladium(II) complex were investigated by NMR techniques. Molecular structures of VOL_2 , NiL_2 , CuL_2 and PdL_2 complexes were determined by single crystal X-ray diffraction technique.



Scheme 1. Synthetic routes for the preparation of the complexes.

The FT-IR spectrum of the complexes exhibits a sharp band around $1600\text{--}1612\text{ cm}^{-1}$, which is assigned to the C=N vibrations of the imine group. This band appeared at 1603, 1611, 1612 and 1612 cm^{-1} for Vanadium(IV), Copper(II), Nickel(II) and Palladium(II) complexes, respectively [33]. The strong band related to the C=O and C=N were observed at the region of 1359 and 1455 cm^{-1} for Vanadium(IV), 1365 and 1459 cm^{-1} for Copper(II), 1366 and

1433 cm^{-1} for Nickel(II) and 1361 and 1434 cm^{-1} for Palladium(II) complexes. Furthermore, absence of the phenolic O–H vibration in complexes is indicative of deprotonation of ligand. Diamagnetic Palladium(II) complex, **PdL₂**, were studied by ¹H and ¹³C NMR experiments (Table 1).

The ¹H and ¹³C NMR were run immediately after solution in DMSO and gave the expected simple spectra, indicating the integrity of the complexes. The spectra obtained after 12, 24 and 120 h were similar to the initial spectra indicating that it is stable in solution. The signal for the imine proton (CH=N) in the Palladium(II) complex appears at 8.8 ppm. The aromatic protons were observed as multiplets in the aromatic region 7.1–8.2 ppm. No signal corresponded to hydroxyl protons suggested the hydroxyl group is fully deprotonated and the oxygen is most likely coordinated to the metal ion. The ¹³C NMR spectrum shows 10 signals for **PdL₂** complex. The peak observed at 164.1 ppm is ascribed to the imine carbon atoms of **PdL₂** complex which supports the presence of the Schiff base in the complex [33].

3.2. Description of the Crystal Structures of Complexes

3.2.1. Structure Description of VOL₂

An ORTEP view of **VOL₂** with the atom-numbering scheme is shown in Fig. 2

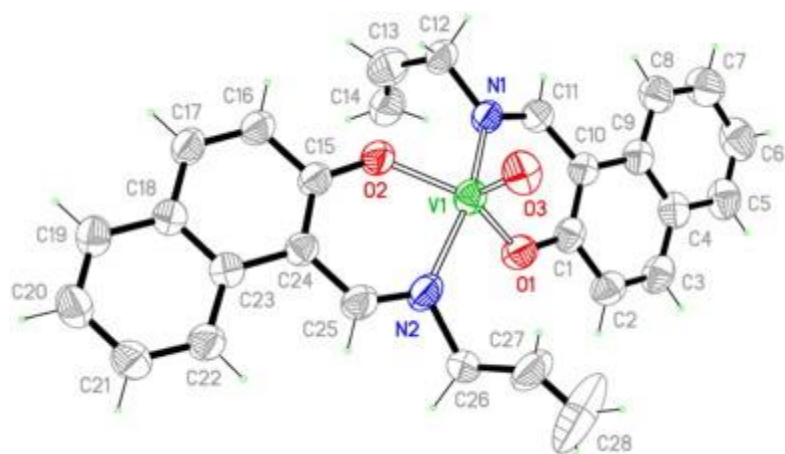


Fig. 2. Perspective view of **VOL₂** in the asymmetric unit showing the numbering scheme. Thermal ellipsoids are drawn at 30% probability level, while hydrogen size is arbitrary.

In this complex, the oxidovanadium(IV) unit is coordinated to two bidentate Schiff base ligands with the two nitrogen and two phenolate oxygen atoms in equatorial positions and one oxygen in the axial position to complete the distorted tetragonal pyramidal N_2O_3 coordination sphere.

The bond angles within the coordination sphere range from $84.53(10)^\circ$ for $O(2)-V(1)-N(1)$ to $85.38(10)^\circ$ for $O(2)-V(1)-N(2)$, which indicates a significant distortion of the

tetragonal pyramid. The $V-O$ [$1.908(2)$ and $1.898(2)$ Å] and $V-N$ [$2.083(3)$ and $2.080(3)$ Å] bond distances in **VOL₂** agree well with the same distances and angles in other

oxidovanadium(IV) Schiff base complexes [38]. The vanadyl ($V-O$) bond length, $1.594(2)$ Å, is similar to this bond in other oxidovanadium(IV) Schiff base complexes [38], [39] and gives a strong absorption in the FT-IR spectrum at 977 cm^{-1} . The two Schiff base ligands coordinate to the vanadium centre in a *trans* geometry with respect to each other. The structural chemistry of small vanadium(IV) molecules is well-established, and, as with vanadium(V), the preponderance of five-coordinate vanadium(IV) complexes adopt a square pyramidal or distorted square pyramidal geometry. To quantitatively compare these structures in terms of their relative geometries about the vanadium atom, we have used the angular structural parameter, τ , which is defined in Scheme S1 [40]. For purely square pyramidal complexes τ is zero. Moving two *trans* ligands out of the equatorial square plane results in a distortion toward a “trigonal bipyramid” for which τ approaches 1 ($\tau = 1$ for a perfect trigonal bipyramid). It should be noted that the symmetry change shown in Scheme S1 is C_{4v} to C_{2v} if all equatorial ligands are equivalent. As reported in other papers [41], [42], we can describe complexes with $0 \leq \tau \leq 0.5$ as distorted square pyramids and with $0.5 \leq \tau \leq 1$ as distorted trigonal bipyramids. A search of the Cambridge Structural Database for monomeric five-coordinate vanadyl complexes with O/N donors yields > 100 structures. A few of them have distorted trigonal bipyramids structure, while most of them have distorted square pyramidal geometry. The paucity of trigonal bipyramids structures for vanadium(IV) suggests that there are electronic and/or steric requirements that preclude the formation of the trigonal bipyramids geometry. According to the above description, the geometry about the our synthesized oxovanadium(IV) Schiff base complex, **VOL₂**, is best described as distorted square pyramidal with $\tau = 0.31$. In the molecular packing of **VOL₂**, three molecules are

connected by intermolecular non-classical [C(17) H(17)⋯ O(3) [2.56(3) Å] C(12) H(12B)⋯ O(3) [2.51(3) Å]] hydrogen bonds (Fig. S1). Additionally, the sum of the weak non-covalent interactions seems to play an important role in the crystal packing and the formation of the framework.

3.2.2. Structure Description of CuL_2

An ORTEP view of CuL_2 with the atom-numbering scheme is presented in Fig. 3 and the crystallographic data and selected bond lengths and angles are collected in Tables 2 and S1. The X-ray structural determination of CuL_2 confirms the assignments of this structure from spectroscopic data. The asymmetric units of CuL_2 contain one-halves of the molecule (Fig. 3)

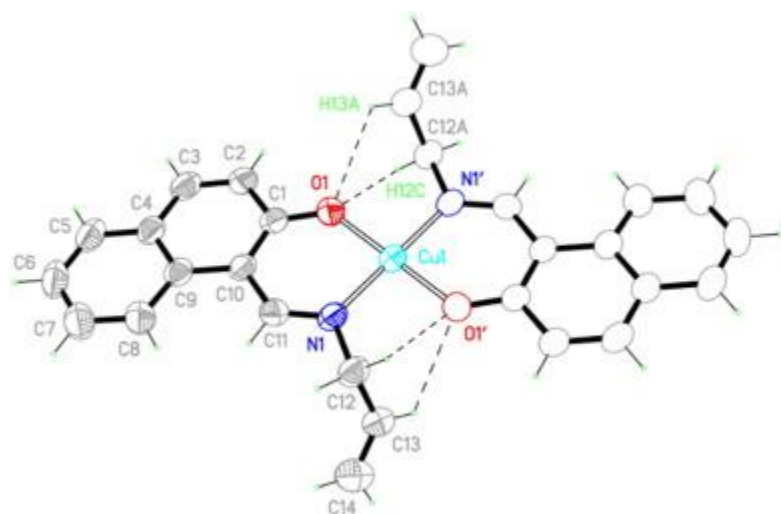


Fig. 3. Perspective view of CuL_2 constituted by the asymmetric unit (filled drawings) showing the numbering scheme and the centrosymmetric half part (empty drawings). Thermal ellipsoids are drawn at the 50% probability level, while the hydrogen size is arbitrary.

Table 2. The HSA binding constant (K_b), the number of binding sites (n), the Stern-Volmer constant (K_{sv}) of the compounds and the quenching rate constant of HSA (k_q).

Compound	K_b/M^{-1}	n	K_{sv}/M^{-1}	$k_q/\text{M}^{-1}\text{S}^{-1}$
VOL_2	5.8×10^4	0.97	5.0×10^4	5.0×10^{12}

Compound	K_b/M^{-1}	n	K_{sv}/M^{-1}	$k_q/M^{-1}S^{-1}$
CuL₂	6.1×10^4	0.75	2.8×10^4	2.8×10^{12}
NiL₂	4.2×10^4	1.0	4.9×10^4	4.9×10^{12}
PdL₂	9.1×10^4	0.8	4.8×10^4	4.7×10^{12}

The Cu atom are located on the inversion centres and surrounded by the two N and the two O atoms of the symmetry related deprotonated 2-hydroxy-1-allyliminomethyl-naphthalen (L⁻) ligand. The four atoms in the equatorial planes around the Cu atom form slightly distorted square-planar arrangements (Table S2).

The hydroxy-1-allyliminomethyl-naphthalen ligands are arranged with respect to each other in a *trans* orientation such that one allyl substituent lies above the [CuO₂N₂] plane and the other below. The Cu—O distances of 1.880(2) Å and the Cu—N bond lengths of 1.998(2) Å are similar to those seen in related complexes [43]. For instance, distances of 1.902(2), 1.896(2) and 2.014(3), 2.003(3)Å for the Cu—O and Cu—N bonds, respectively, are found in a related copper(II) complex derived from allylamine and salicylaldehyde [44].

The C—C distance in **CuL₂** (1.288 (4)) Å is well within the range expected for double bonds found in allyl derivatives. The C—N bond distances is 1.291(4), which are consistent with a slight elongation of the C—N double bond when coordinated to a late metal centre [44]. The allyl groups are centrosymmetric to one another but no significant interaction with a metal centre is observed, thereby allowing access for covalently bond on an insoluble support as heterogeneous catalysts [45].

Although there are no classical hydrogen bonds in the structure, but four intramolecular C—H⋯O contacts are observed in the solid state (Table S3). Intramolecular hydrogen bond occurs between C(12A)—H(12C)⋯O(1) [2.44 Å] atoms and C(13A)—H(13A)⋯O(1) [2.54 Å]

atoms (Fig. 3 and Table S3). In packing of **CuL₂**, the supramolecular aggregations are stabilized by a combination of intermolecular $\pi \cdots \pi$ stacking interactions and $M \cdots \pi$ interactions. π -Stacking interactions between the π -electron clouds of aromatic systems have been extensively observed in many fields such as chemistry [44] and biochemistry [45]. They play an important role in the structures of biological macromolecules [39] and are useful to study on the intercalation of drugs into DNA [46]. The nature of the π -electron is based on $\pi \cdots \pi$ stacking interactions by electron complementarity. The stability order of $\pi \cdots \pi$ stacking is π -electron-deficient- π -electron-deficient $>$ π -electron-deficient- π -electron-rich $>$ π -electron-rich- π -electron-rich [47]. So, the enlargement of π -conjugated systems or polarized perturbation to π -system could change the intermolecular arrangement dramatically. In infinitely π -stacking complexes, solid-state properties such as electrical conductivity depend on the influence of infinite $\pi \cdots \pi$ forces [48]. But the design and synthesis of infinite π -stacking structures, especially supramolecular structures formed by different kinds of π -stacking interactions, are difficult. A selected view of the $\pi \cdots \pi$ interactions and bond parameters is shown in Fig. S2 (Scheme S2). The $\pi \cdots \pi$ interactions exist between Cg(1) \cdots Cg(2), Cg(1) \cdots Cg(4) and Cg(2) \cdots Cg(2) with centroid-centroid distance of 3.8842(17), 3.6347(17) and 3.6684(17) Å, in which Cg(1), Cg(2) and Cg(4) are centres of Cu(1)/O(1)/C(1)/C(10)/C(11)/N(1); C(1)/C(2)/C(3)/C(4)/C(9)/C(10); C(4)/C(5)/C(6)/C(7)/C(8)/C(9) rings, respectively. As depicted in Fig. S2, the π -stacking between aromatic rings have parallel-displaced configurations. The preference parallel-displaced geometry for a $\pi \cdots \pi$ interaction can be understood when keeping in mind the fact that a parallel face-to-face geometry for aromatic rings is not necessarily attractive [49]. Such a parallel or a parallel-displaced π -stacking with a ring separation between 3.3 and 3.8 Å is an important non-covalent organization possibility in supramolecular chemistry [50]. Besides these $\pi \cdots \pi$ interactions, there also exists $Cu \cdots \pi$ interactions between the metal centre of one complex molecule and the phenyl ring of the deprotonated 2-hydroxy-1-allyliminomethyl-naphthalen (L^-) ligand of the other two complex molecules (Fig. S3). This extended $\pi \cdots \pi$ and $Cu \cdots \pi$ interaction seems to be responsible for holding the crystal together. It may be relevant to note here that such non-covalent interactions are of significant importance in molecular recognition processes as well as in crystal engineering [51].

3.2.3. Structure Description of **NiL₂**

The molecular structure of **NiL₂** is shown in Fig. 4. Selected bond distances and angles are listed in Table S2.

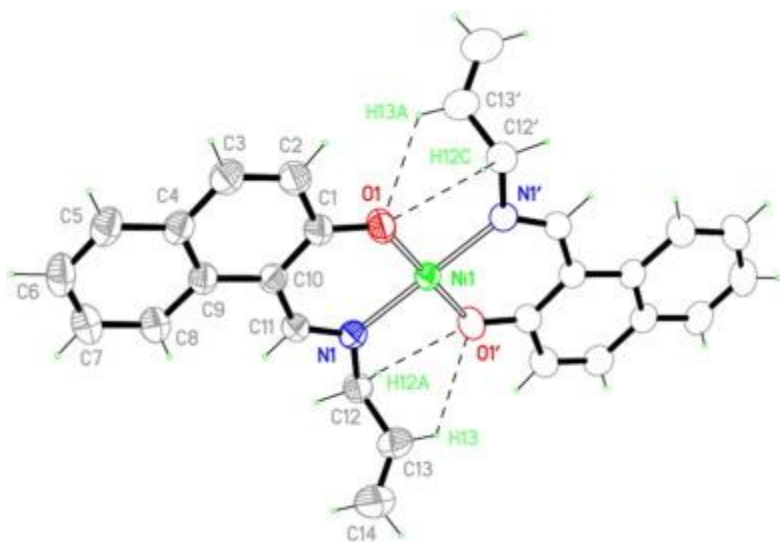


Fig. 4. Perspective view of NiL_2 constituted by the asymmetric unit (filled drawings) showing the numbering scheme and the centrosymmetric half part (empty drawings). Thermal ellipsoids are drawn at the 50% probability level, while the hydrogen size is arbitrary.

The molecular structure of the NiL_2 complex is revealed to be a monomeric complex with an approximately planar configuration about the central nickel centre. The coordination sphere about nickel(II) consists of two phenolato oxygens and two imino nitrogen atoms from two Schiff base ligands, then the nickel(II) ion adopts a slightly distorted square planer geometry. Each Schiff base ligand acts as a chelate using a phenolato oxygen and an imino nitrogen. The deprotonated 2-hydroxy-1-allyliminomethyl-naphthalen ligands are arranged with respect to each other in a trans orientation such that one allyl substituent lies above the $[\text{NiO}_2\text{N}_2]$ plane and the other below. As you can see, NiL_2 and CuL_2 complexes have similar configuration (Fig. 4, Fig. 3). The asymmetric units of NiL_2 and CuL_2 contain one-halves of the molecules. The Ni(1) and Cu(1) atoms are located on the inversion centres and surrounded by the two N and the two O atoms of the symmetry L^- ligands. The four atoms in the equatorial planes around the Ni(1) and Cu(1) atoms form slightly distorted square-planar arrangements (Table S2).

Examination of the main metal–ligand distances shows that the $\text{Ni} \cdots \text{N}$ and $\text{Cu} \cdots \text{N}$ distances are longer than the $\text{Ni} \cdots \text{O}$ and $\text{Cu} \cdots \text{O}$ distance. The $\text{Ni} \cdots \text{N}$ and $\text{Ni} \cdots \text{O}$ distances are 1.993(2) and 1.8889(17) Å for NiL_2 and the $\text{Cu} \cdots \text{N}$ and $\text{Cu} \cdots \text{O}$ distances are 1.998(2) and 1.880(2) Å for CuL_2 , respectively. Typical $\text{Ni} \cdots \text{N}$ and $\text{Cu} \cdots \text{N}$ distances range from 1.904 to 1.922 Å and

from 1.939 to 2.019 Å, while the Ni ... O and Cu ... O distances range from 1.819 to 1.833 Å and from 1.879 to 1.893 Å, respectively [44], [52]. Similar to **CuL₂** complex, two non-classical intramolecular hydrogen bonds of the type C—H ... O are formed between the C—H in the CH₂ and CH groups as donors and O in the 2-hydroxy-1-naphthaldehyde moiety as acceptors (Fig. 4, Table S1). As depicted in Fig. S4 (Scheme S2), in the crystal packing of **NiL₂**, adjacent molecules are assembled through π - π stacking interaction. Centroid-centroid distances between two rings are 3.6992(15) and 3.9275 (16) Å, a typical distance for systems held by π ... π stacking interactions [53]. Also, similar to **CuL₂** complex, there is M ... π interaction in the crystal packing of **NiL₂** complex (Fig. S5). Despite the M ... π interactions are probably weak; however, they are very important in stabilizing the polymeric structure of the complexes. As you can see in Figs. S4 and S5, crystal structure of **NiL₂** contains 1D arrays constructed by the intermolecular π ... π and M ... π interactions. These interactions are responsible for holding the crystal together.

3.2.4. Structure Description of **PdL₂**

An ORTEP view of **PdL₂** with the atom-numbering scheme is presented in Fig. 5 and the crystallographic data and selected bond lengths and angles are collected in Tables 2 and S1. The crystallographic data reveal that the metal centre is four-coordinated by two phenolate oxygen and two imine nitrogen atoms of two Schiff base ligands. The geometry around the metal centre is slightly distorted square planer. The Schiff base ligands are arranged with respect to each other in a *trans* orientation such that two allyl substituents lie on one side of the [MO₂N₂] plane. The Pd

O distance [1.977(5) and 1.980(5) Å] and the Pd—N bond length [1.988(6) and 2.012(5) Å] are similar to those seen in related complexes [54], [55]. For instance, distances of 1.987(3) Å for Pd

O bond and 2.066(3) Å for Pd—N bond are found in a related di-(2-allyliminomethylphenolato)palladium(II) complex derived from allylamine and salicylaldehyde [55].

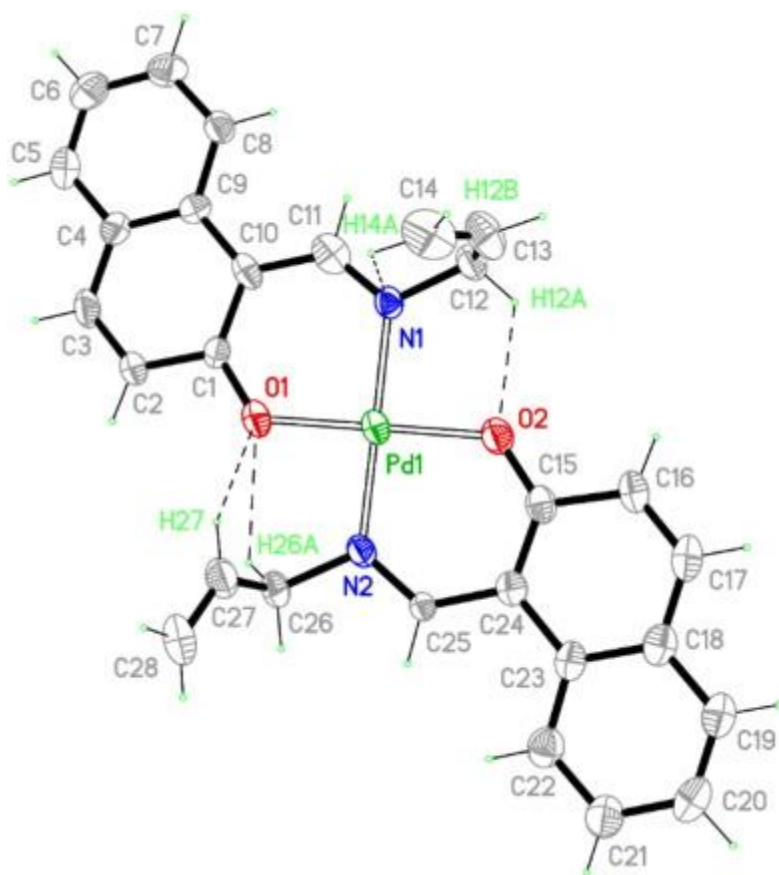


Fig. 5. Perspective view of **PdL₂** constituted by the asymmetric unit (filled drawings) showing the numbering scheme and the centrosymmetric half part (empty drawings). Thermal ellipsoids are drawn at the 30% probability level, while the hydrogen size is arbitrary.

The C—N bond distances are 1.288(9) Å (N1—C11) and 1.325(8) Å (N2—C25), which is consistent with a slight elongation of the C—N double bond when coordinates to a metal centre [44]. The bond angles O—Pd—N [O(1)—Pd(1)—N(2) = 88.6(2)°; O(2)—Pd(1)—N(2) = 91.1(2)°; O(1)—Pd(1)—N(1) = 91.0(2)°; O(2)—Pd(1)—N(1) = 89.2(2)°] are close to 90°. Another interesting feature of the **PdL₂** complex is the presence of interaction between nitrogen atom and hydrogen of allyl group (C14—H14A...N1 [2.575(5) Å]). Recently, we investigated this kind of interaction in Schiff base ligand derived from

allylamine and 2,3-dihydroxybenzaldehyde and its Mo(VI) complex [56]. We suggest the use of pseudo-scorpionate term for this kind of ligand in compliance with the scorpionate ligand exploited for tridentate ligand which would bind to a metal in a fac manner [57].

In order to understanding the nature of scorpion-like intramolecular interaction in the solid state of our reported Schiff base ligand, 3-((*allylimino*)methyl)benzene-1,2-diol, we have performed a series of ab-initio calculation [58]. The energy of the whole rotation around the N1-C8-C9-C10 (θ) torsion angle for one of the two molecules in the asymmetric unit was calculated. During the scan of 360° around θ we observed a series of maximum and minimum points. From the calculated result, we understood that the scorpion like interaction energy trend between hydrogen atom H10A and nitrogen atom N1 appears to be a subtle balance between the H10A \cdots N1 and H9 \cdots N1 interactions and the intramolecular hydrogen bonds O1 \cdots H3 and O1 \cdots H1. A search for salicylideneimine palladium(II) complexes with the Cambridge Structural Database System 2014 showed that except one case [59] the *N,O*-ligand atoms in bis(salicyli-denimine) palladium(II) complexes Pd(*N,O*)₂ adopt a *trans* arrangement in the square planar Pd(II) configuration. As in salen-type complexes Pd(*ONNO*) the *N,O*-ligand atoms are *cis* to each other, they are excluded from the following analysis. The *trans*-Pd(*N,O*)₂ complexes can subdivide into three classes (Scheme S3): planar configuration (with the distance between mean planes of the aromatic rings less than $d = 0.4 \text{ \AA}$) (See for example Refs. [60], [61], [62], [63]), step configuration (with the distance between mean planes of the aromatic rings greater than $d = 0.4 \text{ \AA}$) (See for example Refs. [64]), bowl configuration (See for example Refs. [65], [66]). In the complexes Pd(*N,O*)₂ with planar configuration the Pd atom lies in the plane of the chelate rings (See for example Refs. [60], [61], [62], [63]). The two six-membered chelate rings and their annulated phenyl rings are coplanar (Scheme S3a). The complexes have inversion symmetry. Frequently, however, a characteristic feature of Pd(*N,O*)₂ complexes is an envelope configuration of the six-membered chelate rings with the Pd atom deviating from the plane of the other 5 atoms of the chelate rings. The direct consequence is the alternative of a step or a bowl configuration (Scheme S3b and c). In the step configuration the planes between the aromatic rings are parallel to each other (See for example Refs. [64]). The complexes still have *C_i* symmetry. Some Pd(II) complexes adopt a bowl configuration (See for example Refs. [65], [66]). At best they have *C₂* symmetry. According to the above description, the **PdL₂** complex has planar configuration. As we said in the above sentences, salicylideneimine palladium(II) complexes with planar configuration have inversion centre. But our

palladium(II) complex, **PdL₂**, is the first structure that have planner configuration without inversion centre. Orientation of the two allyl substituents in one side of the [MO₂N₂] plane is the reason of lack of inversion centre in structure **PdL₂** of complex.

3.3. Interaction With Human Serum Albumin (HSA)

3.3.1. UV-vis Absorption

The UV absorption spectrum of HSA shows a strong absorption peak at about 220 nm resulted of the $n \rightarrow \pi^*$ transition for the peptide bond of α -helix and a weak peak at 278 nm assigned to $\pi \rightarrow \pi^*$ transition of the phenyl rings in aromatic acid residues (Trp, Tyr and Phe) [67]. Through addition of various amount of the Schiff base metal complexes (5×10^{-5} M), a hypochromic effect in spectrum of HSA is observed (Fig. 6). This observation indicates that the aromatic amino acid residues of HSA in a hydrophobic cavity were exposed to an aqueous upon binding to the compounds. Moreover, observation of hypochromic effect in UV-vis spectra of HSA with increase amount of the synthesized compounds reveals the π - π stacking interaction between the aromatic rings of the compounds and the phenyl rings of aromatic acid residues [67]. In order to assess the binding ability of the title compounds with HSA, the intrinsic binding constant (K_b) was determined by monitoring the changes of absorbance with increasing concentration of the compounds and using Benesi-Hildebrand plot and the following equation: [68], [69]

$$\frac{1}{(A-A_0)} = \frac{1}{(A_{\max}-A)} + \frac{1}{K_b(A_{\max}-A)} \times \frac{1}{[M]} \quad (3)$$

where A_0 and A are the absorbance of HSA in the absence and presence of drug, respectively. A_{\max} is the obtained absorbance at saturation and $[M]$ is the concentration of drug. The plot of $1/(A - A_0)$ versus $1/[M]$ gives K_b as ratio of y-intercept to slop. The binding constants for **VOL₂**, **NiL₂**, **CuL₂** and **PdL₂** are equal to 4.9×10^4 , 3.5×10^4 , 6.7×10^4 and 9.4×10^4 M⁻¹,

respectively

(Fig. 6).

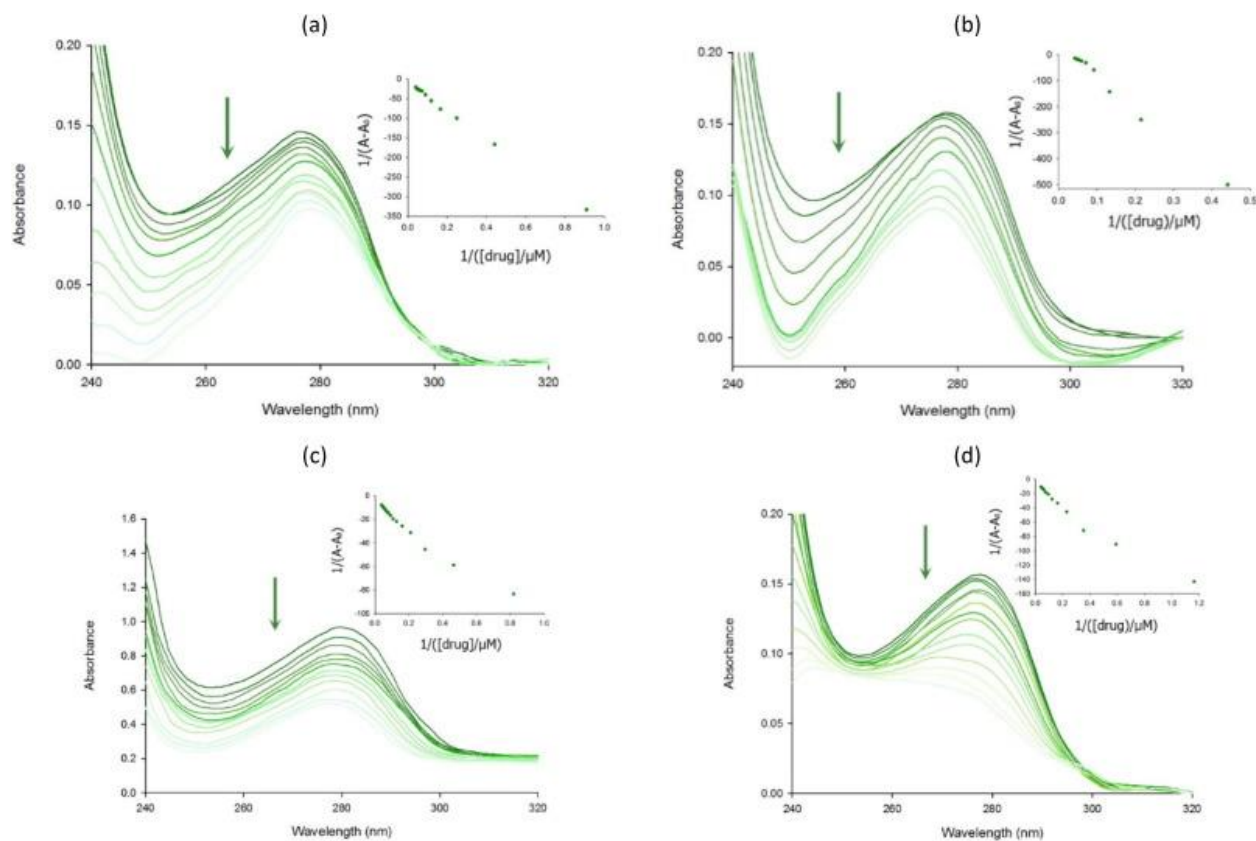


Fig. 6. Electronic absorption spectra of HSA (5 μM) in the absence and presence of various concentrations of (a) VOL₂, (b) NiL₂, (c) CuL₂ and (d) PdL₂ ([compounds] = 0–25 μM).

3.3.2. Fluorescence Spectroscopy

Fluorescence quenching experiment has been performed to obtain information including binding mode, binding constants, number of binding sites and intermolecular distances [70]. Although fluorescence of HSA protein is due to the presence of three amino acids, i.e. tryptophan (Trp), tyrosine (Tyr), and phenylalanine (Phe) residues, the intrinsic fluorescence of HSA comes from tryptophan [71].

The fluorescence intensity of protein was quenched through the addition of the synthesized compounds. This implies that the compounds strongly interact with HSA, leading to changes of microenvironment around the Trp-214 residue in HSA [70], [72]. Fig. 7 represents the fluorescence quenching of 3×10^{-6} M HSA at the presence of various amount of the compounds (5×10^{-5} M).

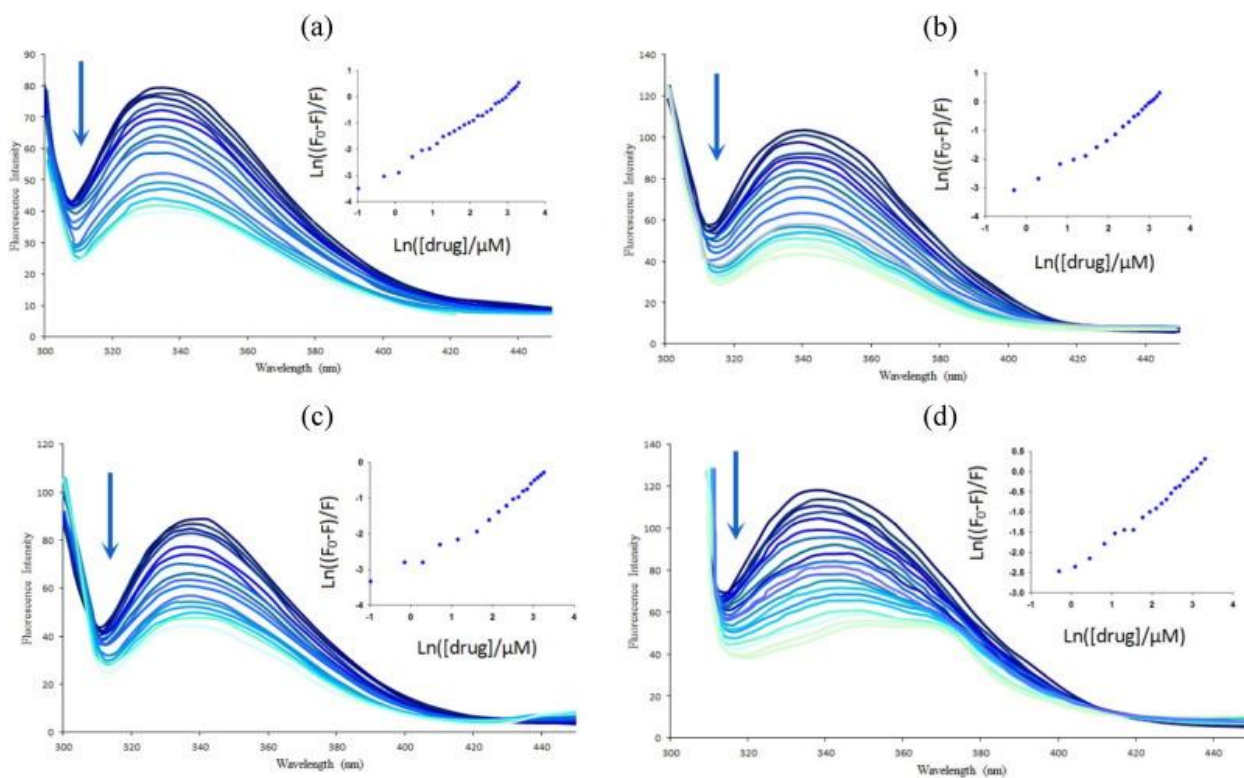


Fig. 7. Changes in the fluorescence spectra of HSA in the presence of (a) **VOL**₂, (b) **NiL**₂, (c) **CuL**₂(d) **PdL**₂. [HSA] = 3 μM , [compound] = 0–25 μM , λ_{ex} = 295 nm.

The absorbance at excitation wavelengths was always < 0.1 , in order to avoid inner filter effects. In order to determine the binding ability between the compounds and HSA, the Stern–Volmer quenching plot was obtained by monitoring the fluorescence quenching of HSA with increasing the concentration of the compounds according to the Stern–Volmer equation: [70]

$$\frac{F_0}{F} = 1 + K_{\text{sv}}[\text{Q}] = 1 + k_{\text{q}}\tau[\text{Q}] \quad (4)$$

where, F_0 and F are the fluorescence intensity of HSA in absence and presence of the compounds. K_{sv} is the Stern-Volmer quenching constant, k_{q} is the quenching rate constant of HSA and τ is the average lifetime of HSA without quencher which is typically equal to 10^{-8} s for biomacromolecules [33]. K_{sv} is determined from the plot of F_0/F vs. $[\text{Q}]$ (Fig. 8). In the present

study, the values of K_{sv} were obtained and presented in Table 2.

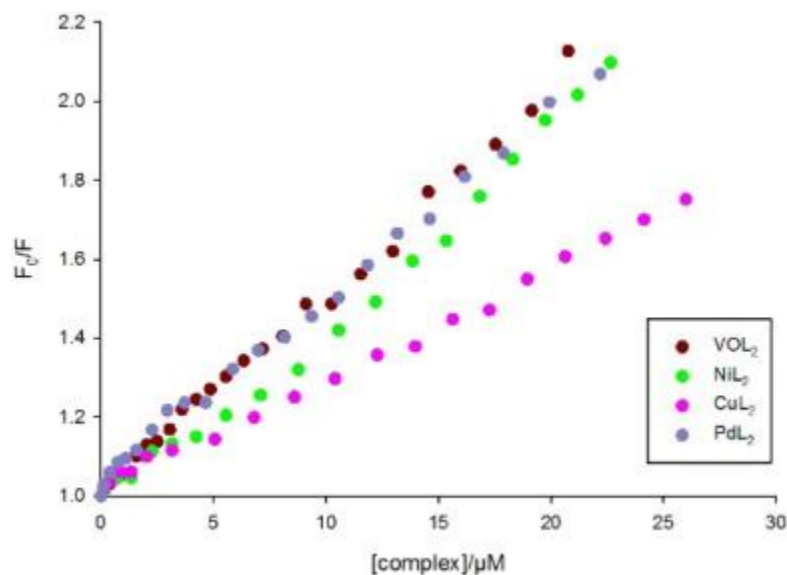


Fig. 8. Stern-Volmer plot for the synthesized compounds–HSA system and the number of binding sites on HAS at room temperature.

Fluorescence quenching is classified to two mechanisms: static quenching and dynamic quenching. In the static mechanism, the fluorophore and the quencher collide together in the ground state while fluorophore and quencher collide together in the excited state in dynamic mechanism. Linearity of the Stern-Volmer plot indicates that quenching fluorescence has only one mechanism, dynamic or static [73].

In this study, the values of kq were obtained and represented in Table 2 that is greater than limiting diffusion rate constant of the diffusional quenching for biopolymers ($2 \times 10^{10} \text{ M}^{-1}\text{S}^{-1}$). This observation supports that quenching fluorescence of HSA occurs by static mechanism [33]. In addition, the changes in the absorption spectrum of HSA shows the formation HSA-drug complex in the ground state, which is because of the change in the HSA structure. While dynamic quenching affects on the excited state and do not have impact on the absorption spectrum.

Moreover, the binding constant (K_b) have been determined using the following equation: [74]

$$\text{Ln}\left(\frac{F_0-F}{F}\right) = \text{Ln}(K_b) + n \text{Ln}[Q] \quad (5)$$

where, F_0 and F are the fluorescence intensity of HSA in absence and presence of Schiff base complex, respectively. $[Q]$ is the concentration of quencher that quencher is the synthesized

compounds here. “ K_b ” is obtained from the plot of $\ln((F_0 - F)/F)$ versus $\ln[Q]$ as a y-intercept. Furthermore, “ n ” which is the number of binding site per protein is slope of the plot. The value of n is nearly 1, indicating that the synthesized compounds bind to HSA with molar ratio of 1:1. The calculated results are shown in Table 2.

The K_b value reveals that the Pd-HSA complex is more stable than other compounds; in the other words this is more available for drug-cell interaction. Moreover, this result is in good agreement with the UV-vis spectroscopy result. In general, binding constant of a drug with a carrier protein such as HSA should be high enough to bind and transfer thought body. Moreover, in order to release a drug since arrival at its target, it should not be too high. With respect to above, HSA-binding constants of all the compounds are in a good range ($2-10 \times 10^4$) [14] and also are comparable to analogue compounds and some potent drugs (Table 3).

Table 3. The value of K_b of some metal complexes and potent drugs.

Compound	K_b (M^{-1})	Ref.	
[Pd(obap)]-	5.56×10^4	[69]	
[Pd(mda)] ²⁻	2.11×10^4	[69]	
PdCl ₂ (N,N-IM)	5.29×10^4	[5]	
Cu(IPA) ₂ (Phen)	1.13×10^4	[74]	
S-ibuprofen	1.1×10^5	[75]	
Anthracycline derivatives	Aclarubicin	4.7×10^3	[76]
	Daunorubicin	2.3×10^3	
	Doxorubicin	2.6×10^3	
	Iododoxorubicin	2.4×10^4	

In addition, our compounds are in the uncharged form which is an advantage for a drug. Because the researches show that the unionized drugs are soluble in lipid and capable of crossing through

the membrane's lipid bilayer while the ionized analogue species fail to cross [75]. The obtained results show that the title compounds with identical ligand and different metal centre bind to HSA differently, confirming the effect of metal ion on affinity of complexes to HSA.

3.3.3. Circular Dichroism (CD) Spectroscopy

CD spectral technique is very effective to diagnose alteration on the secondary structure of HSA causing from HSA–drug interaction and also to investigate the conformation of protein quantitatively. This spectroscopy was performed in the absence and presence of the synthesized metal complexes to prove the impact of them on the secondary structure of HSA. The CD spectra of HSA exhibits two negative peaks at 208 and 222 nm which are characteristic absorption peaks of α -helical structure of protein attributed to the $n-\pi^*$ transfer for the bonds of the α -helix [76]. The band intensities of HSA decreased in negative ellipticity upon the binding of the synthesized complexes to HSA, which indicates the decrease of the α -helical content and increase of disorder structure and β -sheet contents of HSA. This is the result of the formation complex between HSA and the compounds. Moreover, after addition of these compounds the shape of the CD spectra was changed significantly. The results can be expressed in terms of the mean residue ellipticity (MRE) according to Eq. (6): [76]

$$\text{MRE} = \frac{\text{Observed CD (m degree)}}{C_p \cdot nl} \times 10 \quad (6)$$

where, C_p is the molar concentration of protein, l is the path length (0.1 cm), n is the number of amino acid residues that is 585 for HSA. The α -helical contents of free and combined HSA can be calculated from MRE values at 208 nm using the following equation:

$$\alpha - \text{helix}(\%) = \frac{-\text{MRE}_{208} - 4000}{33000 - 4000} \times 100 \quad (7)$$

where, MRE_{208} is the observed mean residue ellipticity value at 208 nm, 4000 is the MRE of the β -sheet and random coil conformation cross at 208, and 33,000 is the MRE value of the pure α -helix at 208 nm. The contents of different secondary structures in HSA are presented in Table 4. As it can be seen, the percentage of α -helix of HSA decreased while those of random coil and β -sheet increased. These results indicate that all the complexes bound to the amino acid residues of

the main polypeptide chain of HSA that causes destroy the original hydrogen bonding networks [77].

Table 4. Changes in the secondary structure of HSA upon its interaction with the synthesized metal complexes in different concentration (R = [compound]/[HSA]).

R	HSA	HSA + VOL ₂			HSA + CuL ₂			HSA + NiL ₂			HSA + PdL ₂		
	0	0.5	1	2	0.5	1	2	0.5	1	2	0.5	1	2
α-Helix	42.9	21.4	14.0	12.4	18.5	13.9	13.4	15.2	16.1	17.0	21.4	13.5	12.4
β-Sheet	30.4	39.6	44.1	44.0	37.4	40.7	42.1	40.3	42.8	44.6	39.6	44.1	44.0
Random coil	26.7	37.8	40.3	43.0	43.0	45.2	43.8	44.2	39.7	38.7	37.8	41.3	43.0

According to the obtained results the maximum capacity of HSA is in molar ratio HSA/drug = 1 and the further addition of compounds caused only minor changes in the CD spectrum. The Fig. 9 represents the changes in the secondary structure of HSA upon addition of the complexes with molar ratio of HSA/complex = 1, indicating the HSA-PdL₂ system has the maximum change that it is based on the magnitude of binding constant of HSA-complex. The obtained results from CD spectroscopy are in a good agreement with fluorescence and UV experiments. The existence of

hydrogen bond between compounds with phenolic hydroxyl group and either C O or N H of the polypeptide chain leads to alter hydrogen bonding network and reduction of protein α -helix structure [78].

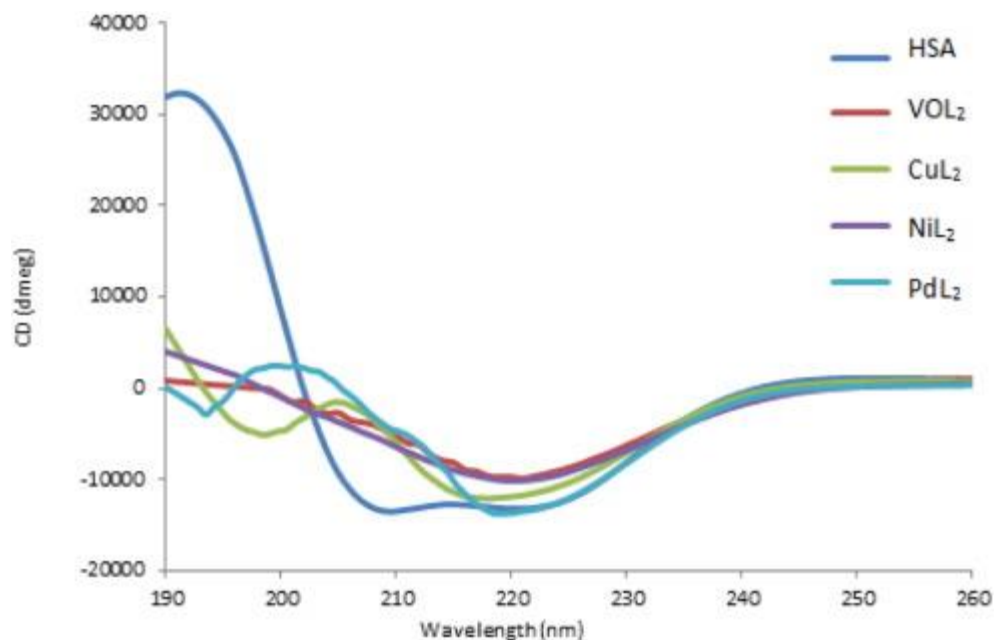


Fig. 9. The CD spectrum of HSA in the absence and presence of the complexes in the molar ratio $[\text{Complex}]/[\text{HSA}] = 1$.

The utilized 2-hydroxy-1-naphtaldehyde in the synthesized metal complexes in this work raises the possibility of this type of hydrogen bond. This is in consistence with the docking results (see section docking study). The observation of considerably reduction in α -helix of HSA in the presence of the synthesized compounds can be as a result of hydrogen bond that can stabilize HSA-compound complex.

3.3.4. Energy Transfer From HSA to Compounds

Energy transfer between the compounds and HSA can provide valuable information about HSA-complex binding. The fluorescence quenching of HSA upon its binding to metal complex can be indicative of energy transfer between HSA and metal complex. This energy transfer can be explained by fluorescence resonance energy transfer (FRET) theory. FRET also known as Förster's resonance energy transfer is an interaction between the excited molecule and its adjacent molecule. Upon this interaction, energy absorbed by donor molecule is transferred to an acceptor [79]. According to this theory, three conditions are required to energy transfer: (1) the donor should have fluorescence, (2) the fluorescence emission spectrum of the donor and the UV–

vis spectrum of the acceptor should have sufficient overlap (3) the small distance between donor and acceptor (< 8 nm) [79]. The distance and efficiency of energy transfer (E) between tryptophan residue of protein (HSA) and drug (complex) has been calculated using this theory through the following equation:

$$E = 1 - \frac{F}{F_0} = \frac{R_0^6}{R_0^6 + r^6} \quad (8)$$

where F_0 and F are fluorescence intensities of HSA in the absence and presence of complex, respectively and R_0 is the critical distance when the transfer efficiency is 50%; r is the distance between donor and acceptor. R_0 can be calculated by Eq. (9)[76].

$$R_0^6 = 8.79 \times 10^{-25} K^2 N^{-4} J \varphi \quad (9)$$

In the above equation, the term K^2 is the orientation factor of the dipoles; N is the refracted index of medium, J is the overlap integral of the fluorescence spectrum of the donor with absorption spectrum of the acceptor and φ is the fluorescence quantum yield of the donor. The value of J can be calculated by the following expression:

$$J = \frac{\sum F(\lambda)\varepsilon(\lambda)\lambda^4 \Delta\lambda}{\sum F(\lambda)\Delta\lambda} \quad (10)$$

where, $F(\lambda)$ is the fluorescence intensity of the donor in the absence of the acceptor at wavelength λ and ε is the molar absorption coefficient of the acceptor at λ . In the present case, $K^2 = 2/3$, $N = 1.336$ and $\varphi = 0.15$ for HSA. Therefore, according to Eqs. (8), (9), (10) the parameters for the synthesized compounds were calculated (Table 5). Fig. 10 represents the overlap of the fluorescence emission spectrum of HSA (5 μ M) and the UV-vis spectrum of **PdL₂** (5 μ M). The related Figs. to **VOL₂**, **NiL₂** and **CuL₂** are shown as Figs. S6 to S8, respectively. The values of r for all the compounds are < 8 nm and $0.5 R_0 < r < 1.5 R_0$, suggesting energy transfer from HSA to the Schiff base metal complexes occurs with high probability. Furthermore, the higher values of r than R_0 , indicating the presence of a static quenching mechanism in the interaction of HSA and compounds [76].

Table 5. The obtained results from FRET theory for the compounds.

Compounds	J ($\text{Cm}^3 \text{L mol}^{-1}$)	R_0 (nm)	r (nm)	E
VOL ₂	6.12×10^{-17}	1.09	1.17	0.39
CuL ₂	3.28×10^{-15}	2.1	2.14	0.47
NiL ₂	9.0×10^{-15}	2.5	2.6	0.44
PdL ₂	1.6×10^{-14}	2.7	2.8	0.45

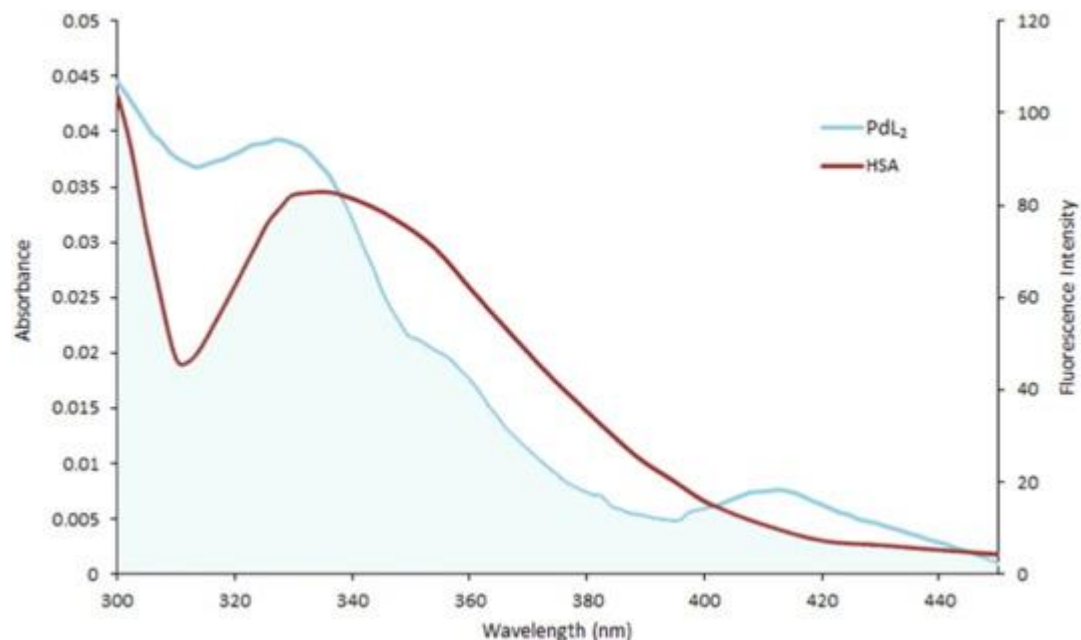


Fig. 10. Spectral overlap of the HSA fluorescence with the **PdL₂** complex absorption spectrum. [HSA] = [PdL₂] = 5 μM , λ_{ex} = 295 nm.

3.3.5. Docking Study

It has been confirmed that the major factor affecting on the distribution, metabolism, the free concentration and the elimination rate of drugs is the binding affinity of drugs to HSA. Moreover, the half-life of drugs depends on their HSA-binding that affects on the dosage of drugs [80]. Therefore the study of interaction between HSA and drug is essential to investigate the pharmacokinetics and availability of drugs in tissues. HSA as the most abundant carrier protein comprises three α -helical domains (I, II and III), each containing two subdomains (A and B) [81]. The previous crystal structure studies showed that many drugs bind to one of the two binding sites located in subdomains IIA and IIIA. However, these sites cannot be responsible for interaction

with all drugs and a large number of endogenous and exogenous compounds bind to the D-shaped cavity in subdomain IB. Zsila reported the subdomain IB as the third major drug binding site on HSA [81]. The primary binding site for hemin, fusidic acid and sulphonamide derivative has been identified site IB. Moreover, researches demonstrated binding of some chemical compounds including dicoumarol, bile acids and biliverdin to this site. The researches revealed that anthracycline antitumor drugs such as doxorubicin and daunorubicin binds to subdomain IB [81], [82].

In this work, the synthesized compounds were docked to the crystal structure of HSA. The obtained results from molecular docking showed that the existence of metal in the compounds triggers the compounds bind to HSA in a suitable orientation and binding site. The appropriate insertion of Pd(II) complex in subdomain IB on HSA was observed with the highest value binding constant. While the other compounds (**VOL₂**, **NiL₂** and **CuL₂**) binds to site IIA that is known as drug site 1. There are a large number of drugs that bind in this site such as warfarin, Amantadine, azapropazone and indomethacin [81]. The results indicated that GLN33, LYS106, TYR148 and ARG186 amino acid residues are involved in the hydrogen bond interaction in the HSA-compound systems. In all the VOL₂-HSA, NiL₂-HSA and CuL₂-HSA systems TYR148 formed hydrogen bond. There is a bifurcated (or three centred) hydrogen bond interaction in the case of **PdL₂** complex between oxygen atom of Pd(II) complex and two hydrogen atom of ARG 186. It should be mentioned that proteins contain a large number of multifurcated hydrogen bonds [83]. The binding energy for **VOL₂**, **NiL₂**, **CuL₂** and **PdL₂** are evaluated - 9.57, - 9.41, - 9.24 and - 7.52 kcal/mol, respectively. The larger negative value of binding energy for **PdL₂** means the higher affinity of it which can be as a result of the existence bifurcated hydrogen bond in PdL₂-HSA system. This result is in a good agreement with experimental data (see related section). The results of docking are presented in Fig. 11, Fig. 12. Moreover, table S4 shows the adjacent amino acids with 3 Å distances to compounds.

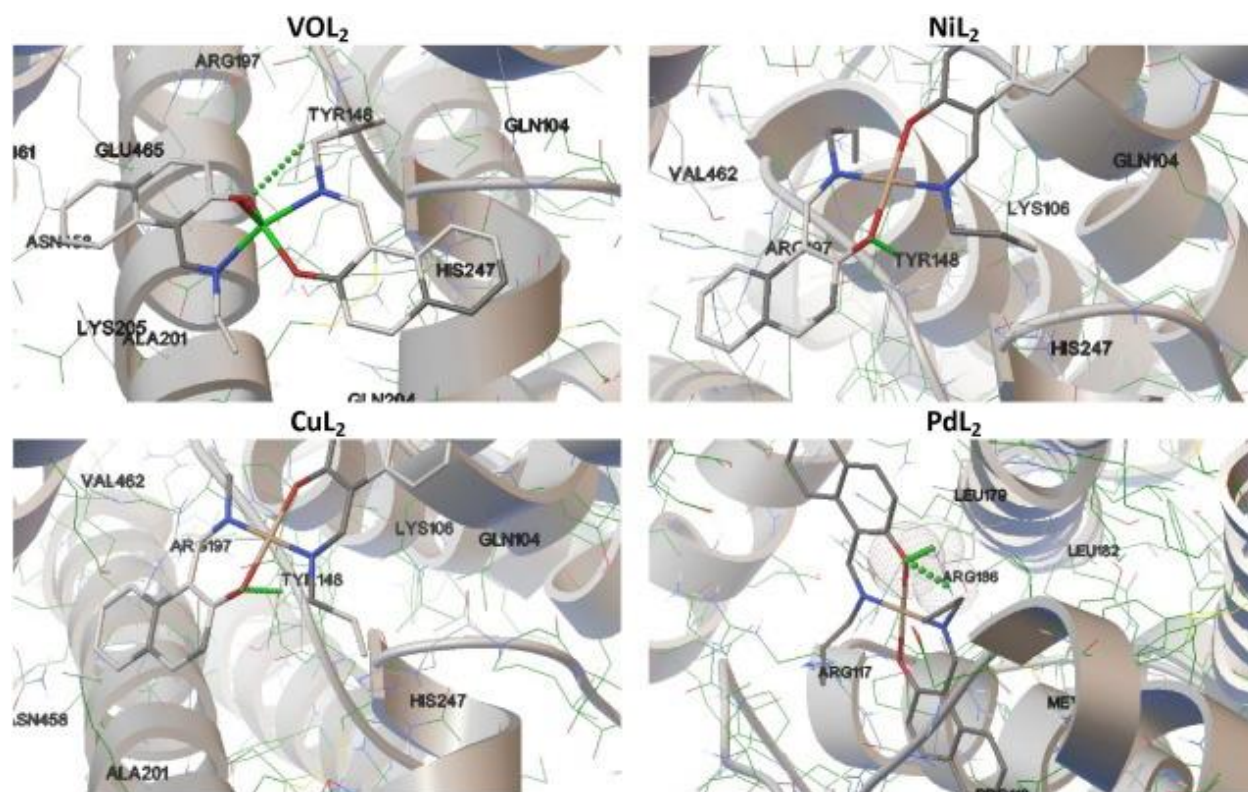


Fig. 11. The docking pose of the synthesized compound-HSA.

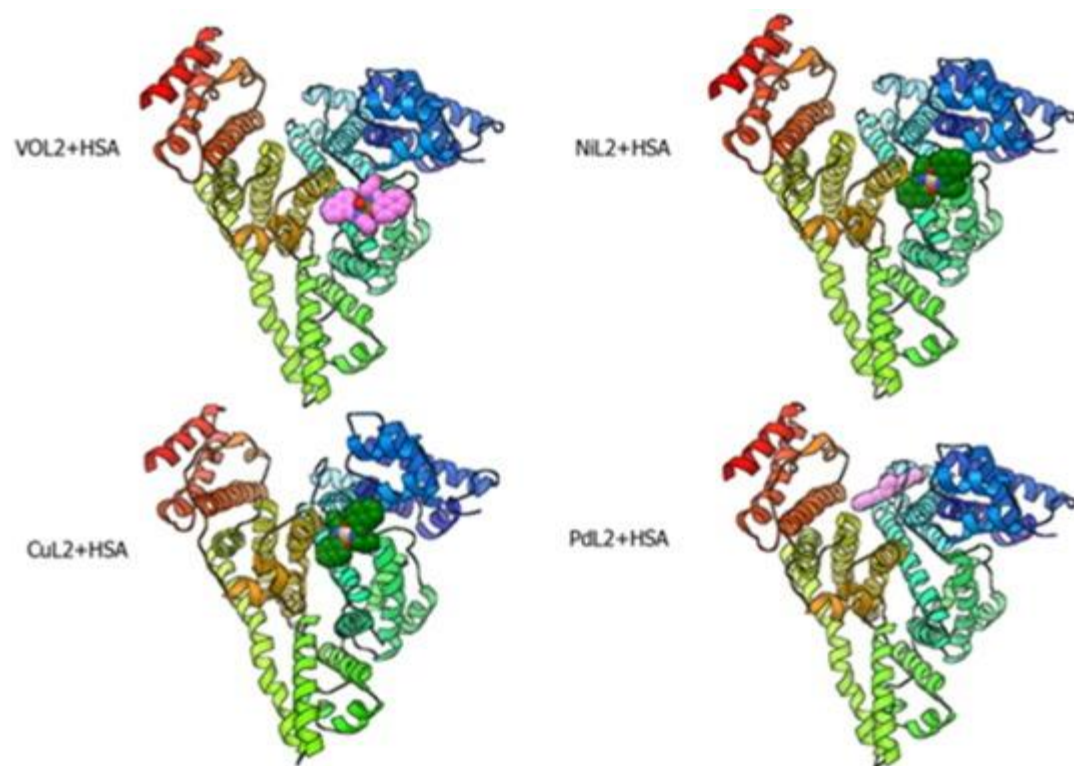


Fig. 12. The docking pose of the synthesized compound-HSA.

3.3.6. QM/MM Calculation

In this work a two-layer ONIOM calculation including (PM6:UFF) was employed to perform QM/MM calculation. The molecular mechanics (MM) was described using the UFF force field for HSA (low layer) while semi-empirical quantum mechanics (QM) method (PM6) was opted for the compounds (high layer). The starting geometry of HSA-compounds for the two layer ONIOM study was obtained from the molecular docking simulation. The geometry was optimized using ONIOM calculation. All calculations were performed using Gaussian 09 quantum chemistry package. All calculations were performed while the structure of HSA and compounds were flexible. The partial atomic charges on the atoms of the compounds and HSA were considered to re-optimize the optimized geometry. In the structure optimization the van der Waals (vdw) and electrostatic interaction were considered. Moreover, the polarization of the wave function of the compounds was considered due to partial atomic charge of HSA in order to obtain more accurate structure [36]. The results of ONIOM indicated that structure of the compounds deviate from the initial geometry due to the binding to HSA. Along with the interaction of the compounds with HSA some bond lengths and bond angles are decreased and/or increased. The existence of these changes can be indicative of the strength of the interaction between HSA and the compounds.

Fig. 13 shows the changes take place in some geometrical parameters including bond lengths and/or bond angles of the compounds along with binding to HSA. The calculated binding energies of the compounds and HSA (ΔE) are about -1.211×10^3 , -1.205×10^3 , -1.259×10^3 and -1.262×10^3 for **VOL₂**, **NiL₂**, **CuL₂** and **PdL₂**, respectively.

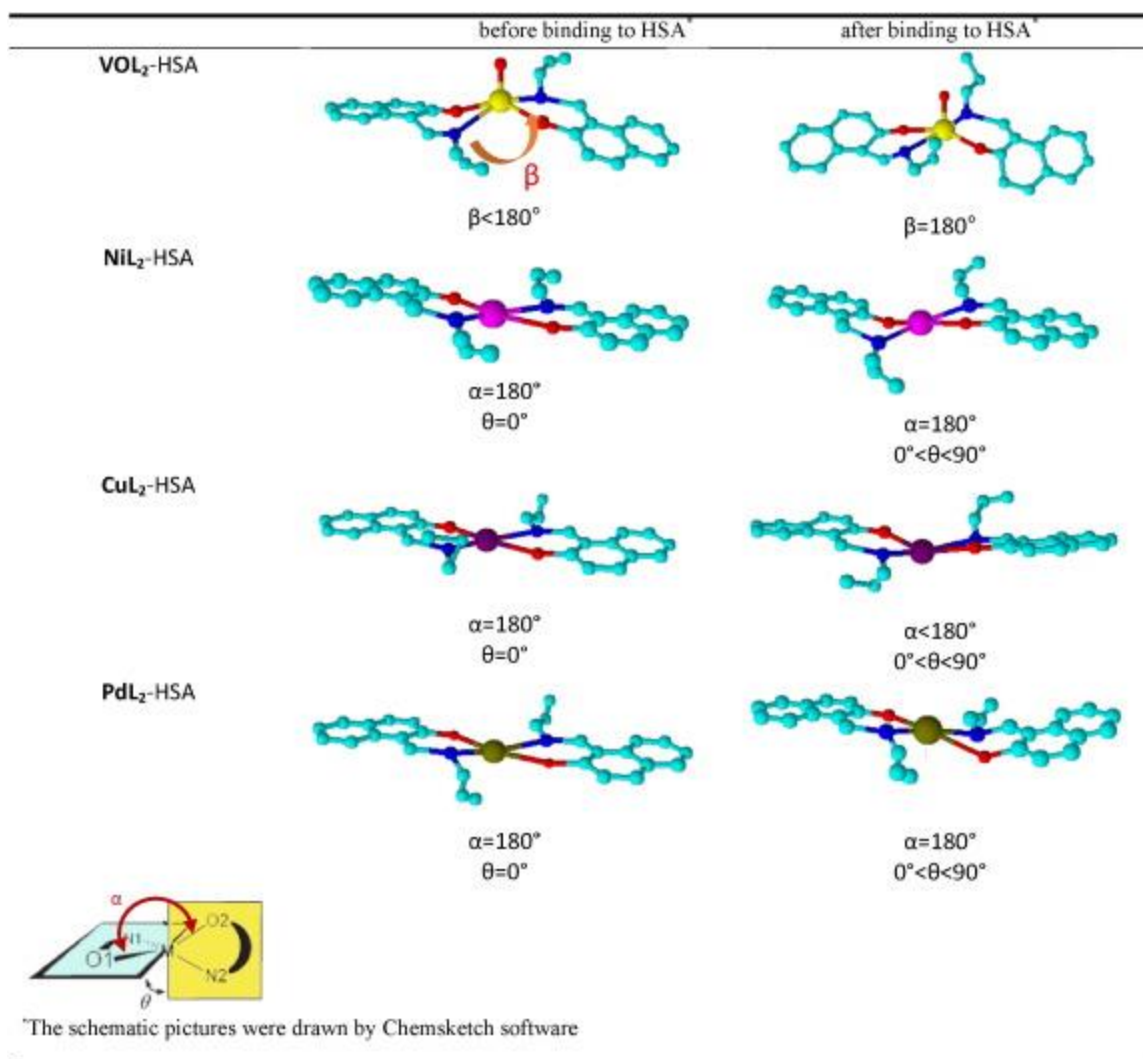


Fig. 13. The structural changes of geometry of the compounds during binding to HSA.

In view of considering the polarization of the compounds in electrostatic field of HSA in QM/MM calculation, this energy is more accurate than that of calculated by docking simulation. The ONIOM calculation reveals that the sequence of affinity of the compounds to HSA is the same as the obtained results from docking calculation and experimental data: **PdL₂** > **CuL₂** > **VOL₂** > **NiL₂**. These results confirm the performed methods in the present study possess reasonable accuracy.

4. Discussion and Conclusions

In the current study, the synthesis of four novel Schiff base metal complexes including Cu(II), Ni(II), Pd(II) and V(IV) has been described. They were characterized by FT-IR, and elemental analysis (CHN). The Schiff base diamagnetic Pd(II) complex were also characterized by ^1H NMR and ^{13}C NMR. Furthermore, their structures were determined by single-crystal X-ray analysis. The crystallographic data show a square planar trans-[MN_2O_2] coordination geometry for the **CuL₂**, **NiL₂** and **PdL₂** complexes while in the **VOL₂**, the vanadium center has a distorted tetragonal pyramidal N_2O_3 coordination sphere. A unique structure for the **PdL₂** was observed in which there is planar configuration without inversion center. The lack of significant interaction between the allyl groups and the metal centres in the complexes allows them to bond on a drug carrier.

The HSA-binding of the synthesized compounds have been evaluated, using experimental (fluorescence quenching, UV-vis spectroscopy and circular dichroism (CD)) and computational methods (molecular docking and QM/MM). The obtained results indicate that the compounds bind to HSA as **PdL₂** > **CuL₂** > **VOL₂** > **NiL₂**. The calculated binding constants between these compounds and HSA were about 3 to $9.5 \times 10^4 \text{ M}^{-1}$. The results of fluorescence experiment as well as the changes in the absorption spectrum of HSA upon addition of the compounds show that the HSA-compound complexes formed in the ground state. In addition, the obtained results from CD spectroscopy indicates upon addition of the synthesized compounds to HSA the percentage of α -helix of HSA decreased while those of random coil and β -sheet increased. Molecular docking studies revealed that hydrogen bond interactions have major role in the interaction of these compounds to HSA. **PdL₂** complex with the highest binding constant interacts with IB site of HSA by formation of three centre hydrogen bond. The ONIOM method was carried out with the aim to investigate more accurately. Based on the ONIOM calculation, the structural parameters of compounds changed due to their interactions with HSA. Generally, the results of the present study exhibit the effect of the metal ion on the HSA-binding whether on the value of binding constant or the binding site.

Acknowledgements

The authors are grateful to the Research Council of the University of Isfahan for financial support of this work.

Appendix A. Supplementary data

Supplementary data to this article can be found online at <http://dx.doi.org/10.1016/j.jphotobiol.2016.07.003>.

References

- [1] J. Ferlay, I. Soerjomataram, M. Ervik, R. Dikshit, S. Eser, C. Mathers, M. Rebelo, D.M. Parkin, D. Forman, F. Bray, Cancer Incidence and Mortality Worldwide, International Agency for Research on Cancer, Lyon, France, 2013.
- [2] M.J. Chow, C. Licon, D.Y.Q. Wong, G. Pastorin, C. Gaiddon, W.H. Ang, Discovery and investigation of anticancer ruthenium–arene Schiffbase complexes via water-promoted combinatorial threecomponent assembly, *J. Med. Chem.* 57 (14) (2014) 6043–6059.
- [3] W. Chen, W. Ou, L. Wang, Y. Hao, J. Cheng, J. Li, Y.-N. Liu, Synthesis and biological evaluation of hydroxyl-substituted Schiff-bases containing ferrocenyl moieties, *Dalton Trans.* 42 (2013) 15678–15686.
- [4] M. Ghosh, M. Layek, M. Fleck, R. Saha, D. Bandyopadhyay, Synthesis, crystal structure and antibacterial activities of mixed ligand copper (II) and cobalt (II) complexes of a NNS Schiff base, *Polyhedron* 85 (2015) 312–319.
- [5] M. Carreira, R. Calvo-Sanjuán, M. Sanaú, X. Zhao, R.S. Magliozzo, I. Marzo, M. Contel, Cytotoxic hydrophilic iminophosphorane coordination compounds of d 8 metals. Studies of their interactions with DNA and HSA, *J. Inorg. Biochem.* 116 (2012) 204–214.
- [6] L. Yan, X. Wang, Y. Wang, Y. Zhang, Y. Li, Z. Guo, Cytotoxic palladium(II) complexes of 8-aminoquinoline derivatives and the interaction with human serum albumin, *J. Inorg. Biochem.* 106 (2012) 46–51.
- [7] V. Joseph, J. Pandya, R. Jadeja, Syntheses, crystal structure and biological evaluation of Schiff bases and copper complexes derived from 4-formylpyrazolone, *J. Mol.*

Struct. 1081 (2015) 443–448.

[8] W. Chu, Y. Wang, S. Liu, X. Yang, S. Wang, S. Li, G. Zhou, X. Qin, C. Zhou, J. Zhang, *Synthesis*,

cytotoxicity and DNA-binding properties of Pd (II), Cu (II) and Zn (II) complexes with 4'-(4-(2-(piperidin-1-yl) ethoxy) phenyl)-2, 2': 6', 2''-terpyridine,

Bioorg. Med. Chem. Lett. 23 (2013) 5187–5191.

[9] J.D. Chellaian, J. Johnson, Spectral characterization, electrochemical and anticancer studies on some metal (II) complexes containing tridentate quinoxaline Schiff base, *Spectrochim. Acta A* 127 (2014) 396–404.

[10] I. Correia, P. Adao, S. Roy, M. Wahba, C. Matos, M.R. Maurya, F. Marques, F.R. Pavan, C.Q. Leite, F. Avecilla, Hydroxyquinoline derived vanadium (IV and V) and copper (II) complexes as potential anti-tuberculosis and anti-tumor agents, *J. Inorg. Biochem.* 141 (2014) 83–93.

[11] A.A. Shoukry, R.M. Alghanmi, Synthesis, DNA binding and complex formation reactions of 3-amino-5, 6-dimethyl-1, 2, 4-triazine with Pd (II) and some selected biorelevant ligands, *Spectrochim. Acta A* 138 (2015) 932–941.

[12] A.R. Kapdi, I.J. Fairlamb, Anti-cancer palladium complexes: a focus on PdX₂L₂, palladacycles and related complexes, *Chem. Soc. Rev.* 43 (2014) 4751–4777.

[13] S. Ramakrishnan, E. Suresh, A. Riyasdeen, M.A. Akbarsha, M. Palaniandavar, Interaction of rac-[M (diimine)₃]²⁺ (M=Co, Ni) complexes with CT DNA: role of 5, 6-dmp ligand on DNA binding and cleavage and cytotoxicity, *Dalton Trans.* 40 (2011) 3245–3256.

[14] M. Kyropoulou, C.P. Raptopoulou, V. Psycharis, G. Psomas, Ni (II) complexes with non-steroidal anti-inflammatory drug diclofenac: structure and interaction with DNA and albumins, *Polyhedron* 61 (2013) 126–136.

[15] C.-Y. Gao, Z.-Y. Ma, Y.-P. Zhang, S.-T. Li, W. Gu, X. Liu, J.-L. Tian, J.-Y. Xu, J.-Z. Zhao, S.-

P. Yan, Four related mixed-ligand nickel (ii) complexes: effect of steric encumbrance on the structure, DNA/BSA binding, DNA cleavage and cytotoxicity, *RSC Adv.* 5 (2015) 30768–30779.

[16] E. Ramachandran, P. Kalaivani, R. Prabhakaran, N.P. Rath, S. Brinda, P. Poornima, V.V.

Padma, K. Natarajan, Synthesis, X-ray crystal structure, DNA binding, antioxidant and cytotoxicity studies of Ni (II) and Pd (II) thiosemicarbazone complexes, *Metallomics* 4 (2012) 218–227.

[17] S.P. Dash, A.K. Panda, S. Pasayat, R. Dinda, A. Biswas, E.R. Tiekink, Y.P. Patil, M. Nethaji, W. Kaminsky, S. Mukhopadhyay, Syntheses and structural investigation of some alkali metal ion-mediated LVVO₂

–(L₂– = tridentate ONO ligands) species:

DNA binding, photo-induced DNA cleavage and cytotoxic activities, *Dalton Trans.* 43 (2014) 10139–10156.

[18] F. Cui, L. Qin, G. Zhang, Q. Liu, X. Yao, B. Lei, Interaction of anthracycline disaccharide with human serum albumin: investigation by fluorescence spectroscopic technique and modeling studies, *J. Pharm. Biomed. Anal.* 48 (2008) 1029–1036.

[19] F. Cui, X. Kong, L. Qin, G. Zhang, Q. Liu, B. Lei, X. Yao, Specific interaction of 4'-O-(αLCladinosyl)

daunorubicin with human serum albumin: the binding site II on HSA

molecular using spectroscopy and modeling, *J. Photochem. Photobiol. B* 95 (2009) 162–169.

[20] S.N. Khan, B. Islam, R. Yennamalli, A. Sultan, N. Subbarao, A.U. Khan, Interaction of mitoxantrone with human serum albumin: spectroscopic and molecular modeling

s[21] Y. Lu, F. Cui, J. Fan, Y. Yang, X. Yao, J. Li, Interaction of human serum albumin with N-(4-ethoxyphenyl)-N'-(4-antipyrinyl) thiourea using spectroscopies and molecular modeling method, *J. Lumin.* 129 (2009) 734–740.

[22] M.M. McCallum, A.J. Pawlak, W.R. Shadrack, A. Simeonov, A. Jadhav, A. Yasgar, D.J. Maloney, L.A. Arnold, A fluorescence-based high throughput assay for the determination of small molecule–human serum albumin protein binding, *Anal. Bioanal. Chem.* 406 (2014) 1867–1875.

[23] F. Li, M. Feterl, J.M. Warner, A.I. Day, F.R. Keene, J.G. Collins, Protein binding by dinuclear polypyridyl ruthenium (II) complexes and the effect of cucurbit [10] uril encapsulation, *Dalton Trans.* 42 (2013) 8868–8877.

[24] C. Domonkos, F. Zsila, I. Fitos, J. Visy, R. Kassai, B. Bálint, A. Kotschy, Synthesis and serum protein binding of novel ring-substituted harmine derivatives, *RSC Adv.* 5

(2015) 53809–53818.

[25] J. Ghuman, P.A. Zunszain, I. Petitpas, A.A. Bhattacharya, M. Otagiri, S. Curry, Structural basis of the drug-binding specificity of human serum albumin, *J. Mol. Biol.* 353 (2005) 38–52.

[26] Y. Gou, Y. Zhang, J. Qi, Z. Zhou, F. Yang, H. Liang, Enhancing the copper (II) complexes cytotoxicity to cancer cells through bound to human serum albumin, *J. Inorg. Biochem.* 144 (2015) 47–55.

[27] C.L. Davies, E.L. Dux, A.-K. Duhme-Klair, Supramolecular interactions between functional metal complexes and proteins, *Dalton Trans.* 10141–10154 (2009).

[28] L.W. Chung, W.M.C. Sameera, R. Ramozzi, A.J. Page, M. Hatanaka, G.P. Petrova, T.V. Harris, X. Li, Z. Ke, F. Liu, H.-B. Li, L. Ding, K. Morokuma, *Chem. Rev.* 115 (2015) 5678.

[29] S. Cie, Program for the Acquisition and Analysis of Data XeAREA, Version 1. 30, Stoe & Cie GmbH, Darmstadt, Germany, 2005.

[30] Stoe&Cie, Program for Data Reduction and Absorption Correction Xe; RED, S.C. GmbH (Ed.), Darmstadt, Germany, 2005.

[31] Stoe&Cie, Program for Crystal Optimization for Numerical Absorption Correction Xe; SHAPE, S.C. GmbH (Ed.), Darmstadt, Germany, 2004.

[32] G.M. Sheldrick, SHELXL97, University of Göttingen, Göttingen, Germany, 1997.

[33] Z. Kazemi, H.A. Rudbari, V. Mirkhani, M. Sahihi, M. Moghadam, S. Tangestaninejad, I. Mohammadpoor-Baltork, Synthesis, characterization, crystal structure, DNA- and HSA-binding studies of a dinuclear Schiff base Zn (II) complex derived from 2-hydroxynaphthaldehyde and 2-picolyamine, *J. Mol. Struct.* 1096 (2015) 110–120.

[34] G.M. Morris, D.S. Goodsell, R.S. Halliday, R. Huey, W.E. Hart, R.K. Belew, A.J. Olson, Automated docking using a Lamarckian genetic algorithm and an empirical binding free energy function, *J. Comput. Chem.* 19 (1998) 1639–1662.

[35] M.I. Dawson, P.D. Hobbs, V.J. Peterson, M. Leid, C.W. Lange, K.-C. Feng, G.-q. Chen, H.L. Jian Gu, S.K. Kolluri, X.-k. Zhang, Y. Zhang, J.A. Fontana, Apoptosis induction in cancer cells by a novel analogue of 6-[3-(1-Adamantyl)-4-hydroxyphenyl]-2-naphthalenecarboxylic acid lacking retinoid receptor transcriptional activation activity, *Cancer Res.* 61 (2001) 4723–4730.

[36] H. Farrokhpour, H. Hadadzadeh, F. Darabi, F. Abyar, H.A. Rudbari, T. Ahmadi-Bagheri,

A rare dihydroxo copper(II) complex with ciprofloxacin; a combined experimental and ONIOM computational study of the interaction of the complex with DNA and BSA, *RSC Adv.* 4 (2014) 35390–35404.

[37] Z.-Q. Liao, C. Dong, K.E. Carlson, S. Srinivasan, J.C. Nwachukwu, R.W. Chesnut, A. Sharma, K.W. Nettles, J.A. Katzenellenbogen, H.-B. Zhou, Triaryl-substituted Schiffbases are high-affinity subtype-selective ligands for the estrogen receptor, *J. Med. Chem.* 57 (2014) 3532–3545.

[38] G. Grivani, V. Tahmasebi, A.D. Khalaji, A new oxidovanadium (IV) complex containing an O, N-bidentate Schiff base ligand: synthesis, characterization, crystal structure determination, thermal study and catalytic activity for an oxidative bromination reaction, *Polyhedron* 68 (2014) 144–150.

[39] A.S.Mahadevi, G.N. Sastry, Cation– π interaction: its role and relevance in chemistry, biology, and material science, *Chem. Rev.* 113 (2012) 2100–2138.

[40] A.W. Addison, T.N. Rao, J. Reedijk, J.v. Rijn, G.C. Verschoor, Synthesis, structure, and spectroscopic properties of copper(II) compounds containing nitrogen–sulphur donor ligands; the crystal and molecular structure of aqua[1,7-bis(Nmethylbenzimidazol-2'-yl)-2,6-dithiaheptane]copper(II) perchlorate, *J. Chem. Soc. Dalton Trans.* 1349 (1984) 1349–1356.

[41] W. Plass, H.P. Yozgatli, Synthesis, reactivity, and structural characterization of dioxovanadium (V) complexes with tridentate Schiff base ligand: vanadium complexes in supramolecular networks, *Z. Anorg. Allg. Chem.* 629 (2003) 65–70.

[42] S.S. Mahajan, M. Scian, S. Sripathy, J. Posakony, U. Lao, T.K. Loe, V. Leko, A. Thalhofer, A.D. Schuler, A. Bedalov, J.A. Simon, Development of Pyrazolone and Isoxazol-5-one Cambinol Analogues as Sirtuin Inhibitors, *J. Med. Chem.* 57 (2014) 3283–3294.

[43] N. Poulter, M. Donaldson, G. Mulley, L. Duque, N. Waterfield, A.G. Shard, S. Spencer, A.T.A. Jenkins, A.L. Johnson, Plasma deposited metal Schiff-base compounds as antimicrobials, *New J. Chem.* 35 (2011) 1477–1484.

[44] M. Khorshidifard, H.A. Rudbari, Z. Kazemi-Delikani, V. Mirkhani, R. Azadbakht, Synthesis, characterization and X-ray crystal structures of vanadium (IV), cobalt (III), copper (II) and zinc (II) complexes derived from an asymmetric bidentate Schiffbase ligand at ambient temperature, *J. Mol. Struct.* 1081 (2015) 494–505.

- [45] C. Baleizão, B. Gigante, H. Garcia, A. Corma, Vanadyl salen complexes covalently anchored to single-wall carbon nanotubes as heterogeneous catalysts for the cyanosilylation of aldehydes, *J. Catal.* 221 (2004) 77–84.
- [46] Y. Shi, M.J. Steenbergen, E.A. Teunissen, L.S. Novo, S. Gradmann, M. Baldus, C.F. Nostrum, W.E. Hennink, *Biomacromolecules* 14 (2013) 1826.
- [47] Q.-L. Ni, X.-F. Jiang, L.-C. Gui, X.-J. Wang, K.-G. Yang, X.-S. Bi, Synthesis, structures and characterization of a series of Cu (I)-diimine complexes with labile N, N'-bis ((diphenylphosphino) methyl) naphthalene-1, 5-diamine: diverse structures directed by π - π stacking interactions, *New J. Chem.* 35 (2011) 2471–2476.
- [48] P. Kar, R. Biswas, Y. Ida, T. Ishida, A. Ghosh, A unique example of structural diversity tuned by apparently innocent o-, m-, and p-nitro substituents of benzoate in their complexes of Mn (II) with 4, 4'-Bipyridine: 1D ladder, 2D sheet, and 3D framework, *Cryst. Growth Des.* 11 (2011) 5305–5315.
- [49] M.O. Sinnokrot, C.D. Sherrill, Substituent effects in π - π interactions: sandwich and Tshaped configurations, *J. Am. Chem. Soc.* 126 (2004) 7690–7697.
- [50] C. Janiak, A critical account on π - π stacking in metal complexes with aromatic nitrogen-containing ligands, *J. Chem. Soc. Dalton Trans.* (2000) 3885–3896.
- [51] S. Burley, G. Petsko, Aromatic-aromatic interactions in and around alpha helices, *Adv. Protein Chem.* 39 (1998) 125–189.
- [52] M.J. Chow, C. Licon, D.Y.Q. Wong, G. Pastorin, C. Gaiddon, W.H. Ang, Discovery and investigation of anticancer ruthenium-arene Schiffbase complexes via waterpromoted combinatorial threecomponent assembly, *J. Med. Chem.* 57 (14) (2014) 6043–6059.
- [53] C.A. Hunter, J.K. Sanders, The nature of pi-pi interactions, *J. Am. Chem. Soc.* 112 (1990) 5525–5534.
- [54] R.R. Coombs, M.K. Ringer, J.M. Blacquiere, J.C. Smith, J.S. Neilsen, Y.-S. Uh, J.B. Gilbert, L.J. Leger, H. Zhang, A.M. Irving, Palladium (II) Schiff base complexes derived from sulfanilamides and aminobenzothiazoles, *Transit. Met. Chem.* 30 (2005) 411–418.
- [55] M. Khorshidifard, H.A. Rudbari, B. Askari, M. Sahihi, M.R. Farsani, F. Jalilian, G. Bruno, Cobalt (II), Copper (II), Zinc (II) and Palladium (II) Schiff base complexes: synthesis, characterization and catalytic performance in selective oxidation of sulfides using

hydrogen peroxide under solvent-free conditions, *Polyhedron* 95 (2015) 1–13.

[56] P. Kalaivani, R. Prabhakaran, F. Dallemer, P. Poornima, E. Vaishnavi, E. Ramachandran, V.V. Padma, R. Renganathan, K. Natarajan, DNA, protein binding, cytotoxicity, cellular uptake and antibacterial activities of new palladium (II) complexes of thiosemicarbazone ligands: effects of substitution on biological activity, *Metallomics* 4 (2012) 101–113.

[57] S. Ponzano, A. Berteotti, R. Petracca, R. Vitale, L. Mengatto, T. Bandiera, A. Cavalli, D. Piomelli, F. Bertozzi, G. Bottegoni, Synthesis, biological evaluation, and 3D QSAR study of 2-methyl-4-oxo-3-oxetanylcarbamic acid esters as N-acylethanolamine acid amidase (NAAA) inhibitors, *J. Med. Chem.* 57 (2014) 10101–10111.

[58] H.A. Rudbari, M. Khorshidifard, B. Askari, N. Habibi, G. Bruno, New asymmetric Schiff base ligand derived from allylamine and 2, 3-dihydroxybenzaldehyde and its molybdenum (VI) complex: synthesis, characterization, crystal structures, computational studies and antibacterial activity together with synergistic effect against *Pseudomonas aeruginosa* PTTC 1570, *Polyhedron* 100 (2015) 180–191.

[59] B.J. Tardiff, J.C. Smith, S.J. Duffy, C.M. Vogels, A. Decken, S.A. Westcott, Synthesis, characterization, and reactivity of Pd (II) salicylaldehyde complexes derived from aminophenols, *Can. J. Chem.* 85 (2007) 392–399.

[60] H. Bahron, A.M. Tajuddin, W.N.W. Ibrahim, S. Chantrapromma, H.-K. Fun, Bis {2-methoxy-6-[(E)-(4-methylbenzyl) iminomethyl] phenolato} palladium (II) chloroform monosolvate, *Acta Crystallogr. Sect. E* 70 (2014) m289–m290.

[61] O.A. Blackburn, B.J. Coe, J. Fielden, M. Helliwell, J.J. McDouall, M.G. Hutchings, Nickel (II) and Palladium (II) complexes of azobenzene-containing ligands as dichroic dyes, *Inorg. Chem.* 49 (2010) 9136–9150.

[62] M.D. Hall, T.W. Failes, D.E. Hibbs, T.W. Hambley, Structural investigations of palladium (II) and platinum (II) complexes of salicylhydroxamic acid, *Inorg. Chem.* 41 (2002) 1223–1228.

[63] T. Tsuno, H. Iwabe, H. Brunner, Synthesis and structural characterization of isomeric palladium (II) complexes with chiral N, O-bidentate ligands, *Inorg. Chim. Acta* 400 (2013) 262–266.

- [64] Z. Gan, K. Kawamura, K. Eda, M. Hayashi, Effect of ortho-substituents on the stereochemistry of 2-(o-substituted phenyl)-1H-imidazoline–palladium complexes, *J. Organomet. Chem.* 695 (2010) 2022–2029.
- [65] A.W. Maverick, R.K. Laxman, M.A. Hawkins, D.P. Martone, F.R. Fronczek, Flexible cofacial binuclear metal complexes derived from α , α -bis (salicylimino)-m-xylene, *Dalton Trans.* (2005) 200–206.
- [66] U. Caruso, R. Diana, B. Panunzi, A. Roviello, M. Tingoli, A. Tuzi, Facile synthesis of new Pd (II) and Cu (II) based metallomesogens from ligands containing thiophene rings, *Inorg. Chem. Commun.* 12 (2009) 1135–1138.
- [67] X.-B. Fu, D.-D. Liu, Y. Lin, W. Hu, Z.-W. Mao, X.-Y. Le, Water-soluble DNA minor groove binders as potential chemotherapeutic agents: synthesis, characterization, DNA binding and cleavage, antioxidation, cytotoxicity and HSA interactions, *Dalton Trans.* 43 (2014) 8721–8737.
- [68] A. Das, G.S. Kumar, Binding studies of aristololactam- β -D-glucoside and daunomycin to human serum albumin, *RSC Adv.* 4 (2014) 33082–33090.
- [69] J.W. Lown, A.V. Joshua, Molecular mechanism of binding of Pyrrolo(1,4)benzodiazepine antitumour agents to deoxyribonucleic acid, *Biochem. Pharmacol.* 28 (1979) 2017–2026.
- [70] E.M. Mrkalić, R.M. Jelić, O.R. Klisurić, Z.D. Matović, Synthesis of novel palladium (II) complexes with oxalic acid diamide derivatives and their interaction with nucleosides and proteins. Structural, solution, and computational study, *Dalton Trans.* 43 (2014) 15126–15137.
- [71] M. Ganeshpandian, R. Loganathan, E. Suresh, A. Riyasdeen, M.A. Akbarsha, M. Palaniandavar, New ruthenium (II) arene complexes of anthracenyl-appended diazacycloalkanes: effect of ligand intercalation and hydrophobicity on DNA and protein binding and cleavage and cytotoxicity, *Dalton Trans.* 43 (2014) 1203–1219.
- [72] Y.-Q. Wang, H.-M. Zhang, G.-C. Zhang, W.-H. Tao, S.-H. Tang, Interaction of the flavonoid hesperidin with bovine serum albumin: a fluorescence quenching study, *J. Lumin.* 126 (2007) 211–218.
- [73] M. Frik, J. Fernández-Gallardo, O. Gonzalo, V. Mangas-Sanjuan, M. González-Alvarez,

- A.S.d. Valle, C. Hu, I. González-Alvarez, M. Bermejo, I. Marzo, M. Contel, Cyclometalated iminophosphorane gold(III) and platinum(II) complexes. A highly permeable cationic platinum(II) compound with promising anticancer properties, *J. Med. Chem.* 58 (15) (2015) 5825–5841.
- [74] S.U. Dighe, S. Khan, I. Soni, P. Jain, S. Shukla, R. Yadav, P. Sen, S.M. Meeran, S. Batra, Synthesis of β -carboline-based N-heterocyclic carbenes and their antiproliferative and anti-metastatic activities against human breast cancer cells, *J. Med. Chem.* 58 (8) (2015) 3485–3499.
- [75] O.K. Abou-Zied, Revealing the ionization ability of binding site I of human serum albumin using 2-(2'-hydroxyphenyl) benzoxazole as a pH sensitive probe, *PCCP* 14 (2012) 2832–2839.
- [76] Y. Huang, S. Wang, Y. Bi, J. Jin, M.F. Ehsan, M. Fu, T. He, Preparation of 2D hydroxyrich carbon nitride nanosheets for photocatalytic reduction of CO₂, *RSC Adv.* 5 (2015) 33254–33261.
- [77] P. Banerjee, S. Ghosh, A. Sarkar, S.C. Bhattacharya, Fluorescence resonance energy transfer: a promising tool for investigation of the interaction between 1-anthracene sulphonate and serum albumins, *J. Lumin.* 131 (2011) 316–321. *studies, Eur. J. Pharm. Sci.* 35 (2008) 371–382.
- [78] M.-X. Xie, X.-Y. Xu, Y.-D. Wang, Interaction between hesperetin and human serum albumin revealed by spectroscopic methods, *Biochim. Biophys. Acta Gen. Subj.* 1724 (2005) 215–224.
- [79] N. Fani, A. Bordbar, Y. Ghayeb, A combined spectroscopic, docking and molecular dynamics simulation approach to probing binding of a Schiff base complex to human serum albumin, *Spectrochim. Acta A* 103 (2013) 11–17.
- [80] S. Ranjbar, Y. Shokohinia, S. Ghobadi, N. Bijari, S. Gholamzadeh, N. Moradi, M.R. Ashrafi-Kooshk, A. Aghaei, R. Khodarahmi, Studies of the interaction between isoimperatorin and human serum albumin by multispectroscopic method: identification of possible binding site of the compound using esterase activity of the protein, *Sci. World J.* 2013 (2013).
- [81] F. Zsila, Subdomain IB is the third major drug binding region of human serum albumin: toward the three-sites model, *Mol. Pharm.* 10 (2013) 1668–1682.

[82] F. Zsila, Circular dichroism spectroscopic detection of ligand binding induced subdomain IB specific structural adjustment of human serum albumin, *J. Phys. Chem. B* 117 (2013) 10798–10806.

[83] T. Steiner, The hydrogen bond in the solid state, *Angew. Chem. Int. Ed.* 41 (2002) 48–76.